UNIVERSITAT POLITÈCNICA DE VALÈNCIA

Escuela Técnica Superior de Ingeniería del Diseño

UNIVERSITAT POLITÈCNICA DE VALÈNCIA

School of Design Engineering

Hydrofoil design for surfboard

End of Degree Project

Bachelor's Degree in Aerospace Engineering

AUTHOR: Alcañiz Brull, Néstor

Tutor: Margot, Xandra Marcelle

ACADEMIC YEAR: 2022/2023

1 Abstract

Along this project two different designs of a surfboard's hydrofoil for kitefoiling are developed following different requirements, the first one is designed for beginners, prioritizing stability and lift generation, while the second one is focused in professionals, prioritizing maneuverability and the capability of reaching higher velocities. Both of these designs are validated by means of a computational fluid dynamics simulation using the commercial software Star CCM+. The main forces (lift and drag) and the pitching moment generated are calculated for different velocities and angles of attack and roll and the flow behaviour is studied in detail, analyzing how the geometries affect the fluid by means of vorticity and velocity contours and pressure coefficient plots. Finally, it is concluded that the geometries fulfill the requirements established.

A lo largo de este proyecto se desarrollan dos diseños diferentes de hydrofoils para tablas de surf para kitefoiling siguiendo diferentes requerimientos, el primero está diseñado para principiantes, priorizando la estabilidad y la generación de sustentación, mientras que el segundo está centrado en profesionales, priorizando la maniobrabilidad y la capacidad de conseguir altas velocidades. Ambos diseños son validados mediante cálculo de fluidos computacional utilizando el programa comercial Star CCM+. Las fuerzas principales (sustentación y resistencia) y el momento de cabeceo generados se calculan para diferentes velocidades y ángulos de ataque y alabeo y el comportamiento del fluido se estudia en detalle analizando como las geometrías afectan al fluido mediante contornos de vorticidad y velocidad y gráficos de coeficiente de presiones. Finalmente, se concluye que las geometrías cumplen con la lista de requisitos establecida.

Contents

2 Introduction

Hydrofoils have many different applications, most of them related with boats efficiency increase, but recently a new trend has emerged which consists in joining these hydrofoils to kitesurf boards. This has created a whole new sport called kitefoiling.

This project consists in developing two hydrofoils designs for this new sports following two different tendencies. One design is a better option for beginners, able to obtain more lift at lower velocities and prioritizing the stability in order to make it easier to learn how to practise this sport, and the other design aims for higher maneuverability and maximum reachable speed, switching the focus to professionals who are looking to compete in this new sports, either in races or acrobatic competitions. This designs are created in order to provide a new model to the market and contribute in the expansion of this new sport by either giving the opportunity of practising it by means of creating a design that eases the initiation in this sport, making it less frustrating for the beginners, or by giving the opportunity to reach a new competitive level by means of a design that allows the pilot to exploit his or her full potential.

The methodology followed consists in creating a list of requirements for each case as a base and developing a geometry that fulfills that list. For checking if the requirements are fulfilled and the designs' performance, different scenarios are simulated by means of computational fluid dynamics in order to analyze how the geometry affects the fluid. First a sweep of lift, drag and pitching moment at different velocities is calculated in order to obtain a relation between lift and velocity. Once this relation is obtained, the velocity needed to reach an equivalent lift to 70 kilos is calculated and at this velocity the fluid behaviour is analyzed at zero degrees of angle of attack and zero degrees of roll and at zero degrees of angle of attack but 15^{o} of roll. Lastly, both angle of attack and velocity are changed in order to obtain the same lift but at a lower velocity.

3 State of the Art

In the recent past, the hydrofoils' applications to water sports have increased significantly creating a whole new market which attends the demands of an increasing number of users who prefer the experience a hydrofoil can create. This market has been supplied by different companies which lead the innovations in the sector and continuously innovate and develop new designs, aiming to reach every possible customer, beginner or expert. The most relevant companies at the moment are Armstrong Foils, Lift Foils, Cabrinha and Gong.

About the designing tendencies, the latest innovations in the industry always try to achieve a maximum efficiency and comfort for the pilot and tend to reach as many customers as possible, both beginners and experts. The newest tendencies show an increase in the main wing aspect ratio to values of around 10 to 15 (as seen in the newest Armstrong Foils' models [1], seen in Figure 1) and a reduction in size of the secondary wing in order to reduce the drag generated.

Figure 1: Armstrong foil kit HA525

Moreover, some companies such as Gong [2] or Cabrinha [3], seen in Figure 2 and Figure 3, try to make the foiling experience more comfortable for the pilot by offering a wide range of adjustable designs, allowing the pilot to adjust the angle of attack and the fuselage's length, making him or her able to create the ideal geometry for each ride.

Figure 2: Gong foil kit Allvator v2 x-over

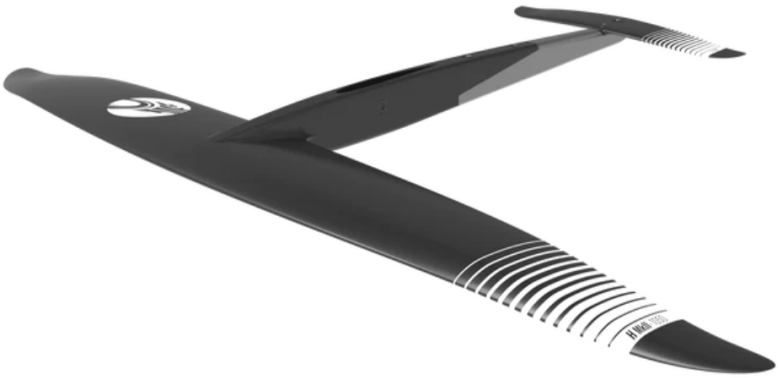

Figure 3: Cabrinha foil kit fusion H

Lift Foils [4] is trying to differentiate itself from the rest of the competitors by creating a so called eFoil, seen in Figure 4, which is a common hydrofoil design which includes an electric engine, making the pilot able to adjust the velocity at will without depending on the wind's speed or the kite's size, making, once again, a more comfortable experience for the pilot.

Figure 4: Lift eFoil kit LIFT4

This designing innovations are supported by the development of new manufacturing methods such as the study in composite materials and the 3D printing, which allows to manufacture more complex shapes in a highly accurate way, allowing the designers to create more complex geometries. The newest tendencies in manufacturing methods are related to the carbon fiber manufacturing due to its stiffness, which can be seen in both of the wings in all of the newest models from the companies mentioned beforehand.

4 Base Geometry and Meshing

4.1 Base Geometry

The project's initial point is a base geometry which will be used to develop the meshing process and mesh independence study. This base geometry is a variation of an online model [5] and consists in two wings joined by a cylindrical body as seen in Figure 5. The line shown in Figure 6 marks the symmetry plane. The simulations and studies will be performed using only one half of the geometry in order to reduce the computational cost.

Figure 5: Base geometry side view

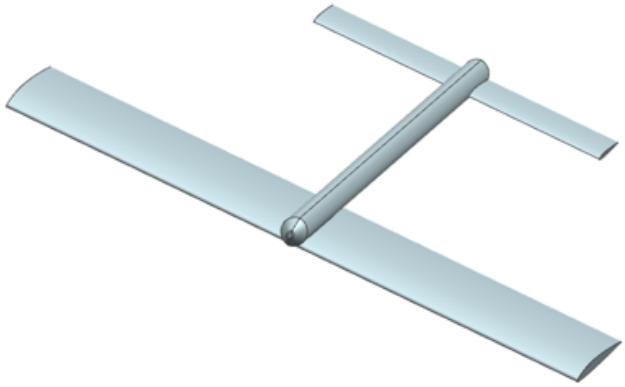

Figure 6: Base geometry perspective view

This base geometry's performance will not be studied since it is not a model designed by the author. It will only be used in order to perform the mesh independence study.

4.2 Meshing

The meshing process consists in creating the desired control volumes and dividing them into several cells of the needed size.

For this study, several control volumes have been created in order to obtain a more refined mesh in the more critical zones (around the body and in the wake sections) without increasing

the amount of cells in less critical zones thus reducing the computational cost without affecting the calculus' precision.

The main control volume consists in a bullet shaped figure which extends the length of seven main wing's chords upstream from the main wing's leading edge and ten main wing's chords downstream from the secondary wing's trailing edge. The volume radius is five times the geometry's half span. This dimensions have been chosen in order to ensure that the boundary conditions needed to perform the simulations are properly established and coherent with the case studied, avoiding problems when simulating. This kind of shape is chosen among a regular box because of the lack of interest in the corners of the volume. Note that, since just half of the geometry is going to be simulated, the volume has a symmetry plane.

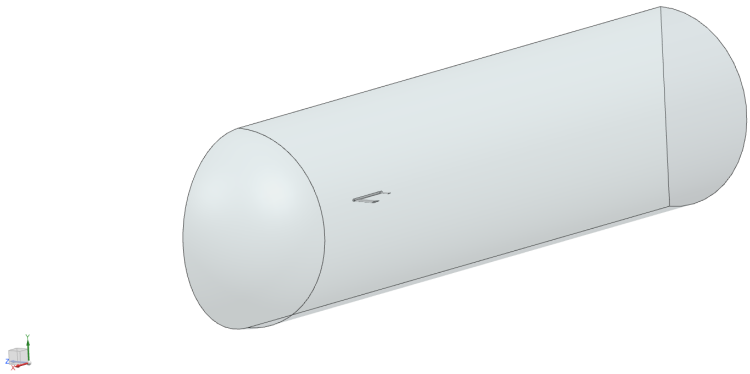

Figure 7: Main control volume perspective view

In addition to the control volume seen in Figure 7, other control volumes were created as getting closer to the most critical zones, which are the geometry itself and the wake generated. The bigger one, seen in Figure 8 encloses the whole geometry leaving a main wing's chord upstream and with a width of three times the half span. The length downstream is not as important since more control volumes will be created extending downstream.

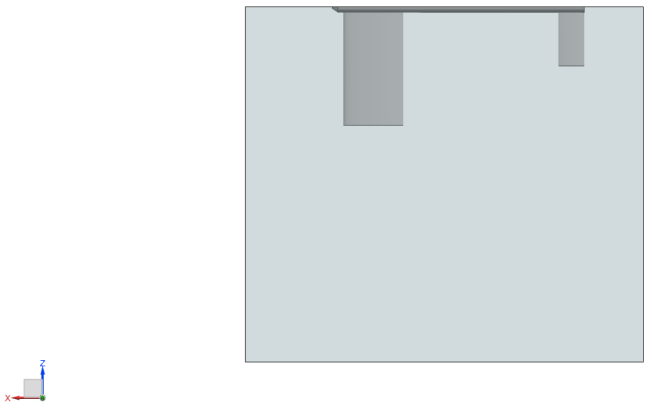

Figure 8: Second control volume

Apart from the volume seen in Figure 8, three more volumes, seen in Figure 9 were created enclosing the main wing, its wake and the wake of the secondary wing. Since the secondary wing is in the wake of the first one, no additional volume was created. The volume created for the main wing extends the main wing's chord in length and three times its span in width. The volume created to enclose the wake of the main wing extends between both of the trailing edges and the last volume, created to enclose the secondary wing's wake extends from its trailing edge to five times the main wing's chord. The three volumes have the same width as seen in Figure 9.

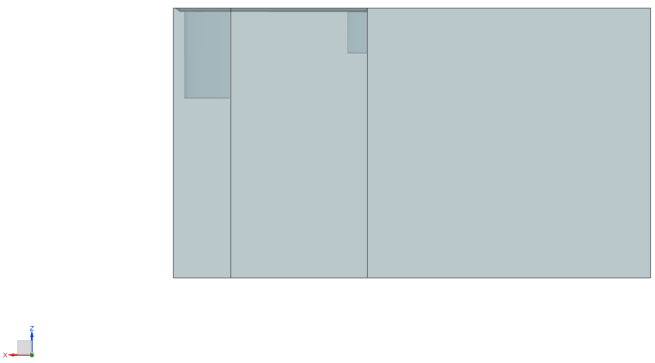

Figure 9: Main wing and both wakes control volume

The cells' size used for the volume seen in Figure 7 will be in any case the biggest one, followed by the volume seen in Figure 8. The most refined mesh will be in the three volumes seen in Figure 9, reducing the cell size from left to right, since it is the flow direction and the wake zones are more critical.

To sum up, in Figure 10 and Figure 11 the five volumes created can be seen from a side point of view and in perspective.

Figure 10: Control volumes' side view

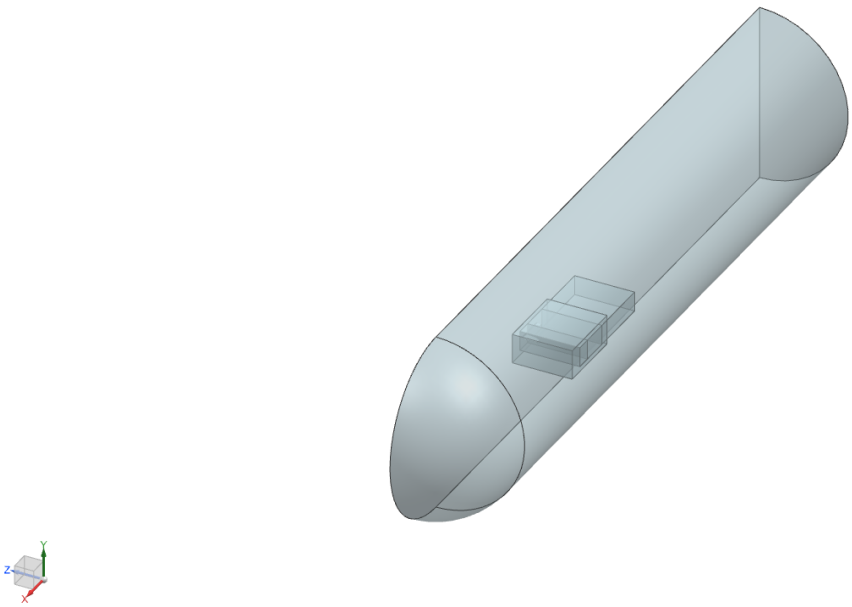

Figure 11: Control volumes' perspective view

Moreover, the boundary layer has to be defined by means of a prism layer meshing. In this case, the prism layer's total thickness has been established to be a 10% of the body's thickness, being the reference the main wing's profile maximum thickness for the first one and the secondary wing's profile maximum thickness for the second one. Although the fuselage also extends in the second volume seen from left to right in Figure 9, the size chosen is not the

fuselage's radius since the most critical part is the secondary wing. For the last volume no boundary layer is needed since there is no body to be meshed contained in that volume.

5 CFD Set Up

5.1 Set Up

The first step is to define the media in where the simulation has to be performed, in this case, seawater. In order to establish the properties of seawater, the average salinity is assumed to be at 35 parts per million and the average temperature to be 298 Kelvin [6]. The fluid has been modeled as a constant density fluid and the properties used for the set up of the simulation are shown in Table 1, measured in the international system's units.

	Value	Units
Dynamic viscosity	0.000959	$[Pa \cdot s]$
Density	1023.6	$[\frac{kg}{m^3}]$

Table 1: Seawater properties

The simulations are performed in 3D and in a steady temporal regime, focusing in the cruise navigation. The solver selected is a segregated solver since the seawater has constant density and the viscous regime has been defined as turbulent. About the turbulence, the k-ω turbulence model is used and they are solved following the Reynolds-Averaged Navier-Stocks method.

In order to perform a proper meshing it is crucial to establish the needed boundary conditions since the mesh depends on them. In this case, the boundary conditions have been applied to the volume control seen in Figure 7. The faces seen in Figure 12 are defined as a symmetry plane for the blue face and a pressure outlet for the orange one. The missing face to create the control volume seen in Figure 7 is defined as a velocity inlet.

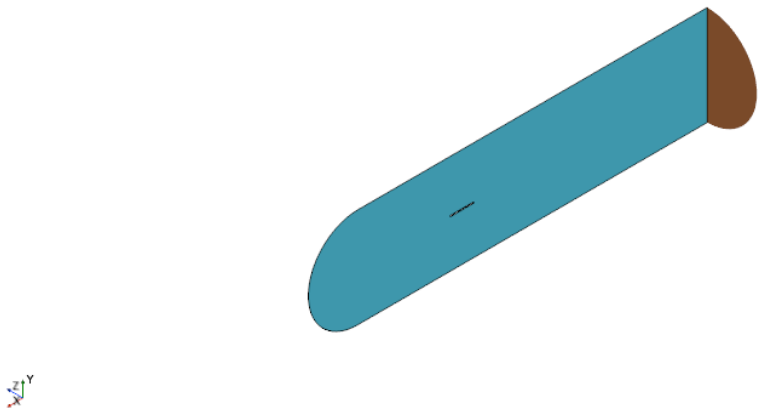

Figure 12: Main control volume's symmetry plane and outlet

The conditions established for the inlet and the outlet are shown in Table 2, where the velocity has been defined to go parallel to the x axis towards the outlet.

Inlet Conditions	Outlet Conditions
$v_{inf} = 20\ knts = 10.29\ m/s$	$p = 101325$ Pa

Table 2: Boundary conditions

The initial conditions have been set up to be coherent with the inlet and outlet conditions seen in Table 2. The velocity value of the inlet condition will be varied over the course of the document in order to perform the analysis of the geometries designed.

5.2 Convergence Criteria

One of the most important steps in the Computational Fluid Dynamics methodology consists in obtaining a converged simulation, this is, to ensure that the simulation performed by the computer reaches an accurate solution.

For considering a simulation converged different criteria has to be accomplished. In this case, the residuals must achieve a magnitude of 10^{-6}. Moreover, the drag variation must be less than 0.01 and the lift variation less than 0.1 between iterations. Once all this criteria has bee accomplished, the solution is considered as converged and, therefore, acceptable to study.

The implementation of this criteria can be seen in Figure 13, Figure 14 and Figure 15, all images obtained from a simulation performed when obtaining the mesh independence. The Figure 13 show the evolution of the residuals along the different iterations and Figure 14 and Figure 15 sow the evolution of the lift and drag forces calculated in each iteration.

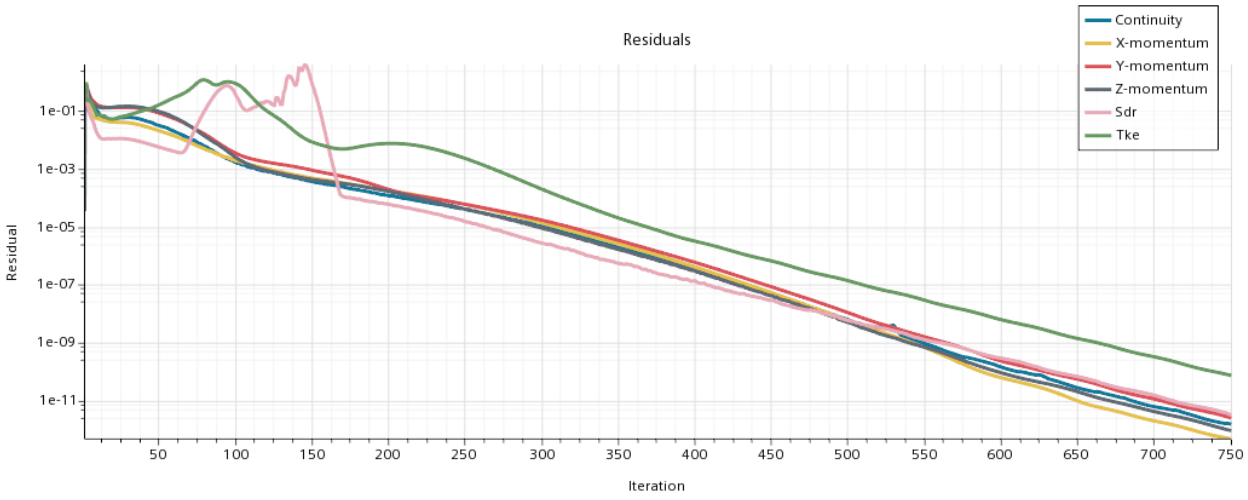

Figure 13: Simulation residuals

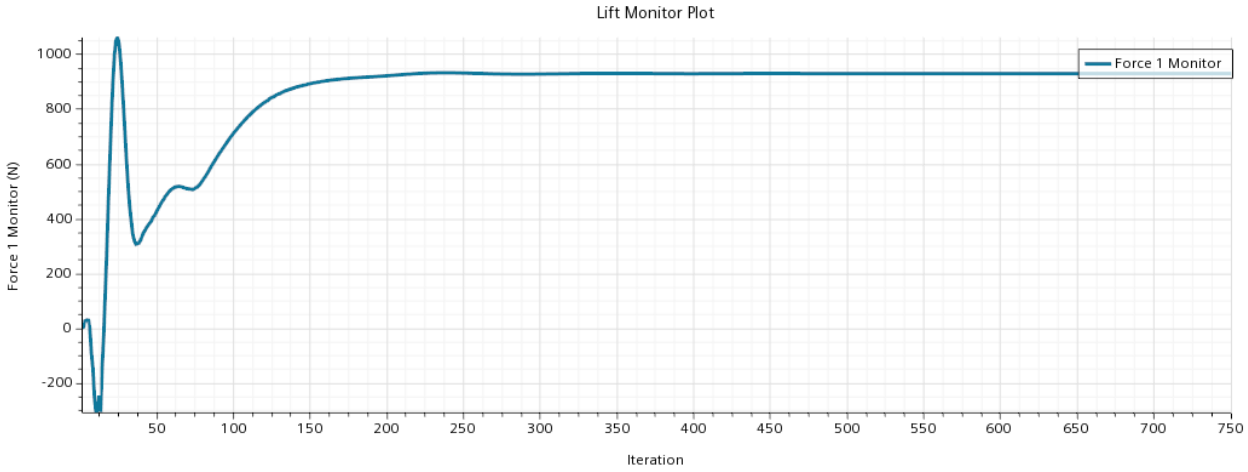

Figure 14: Lift monitor plot

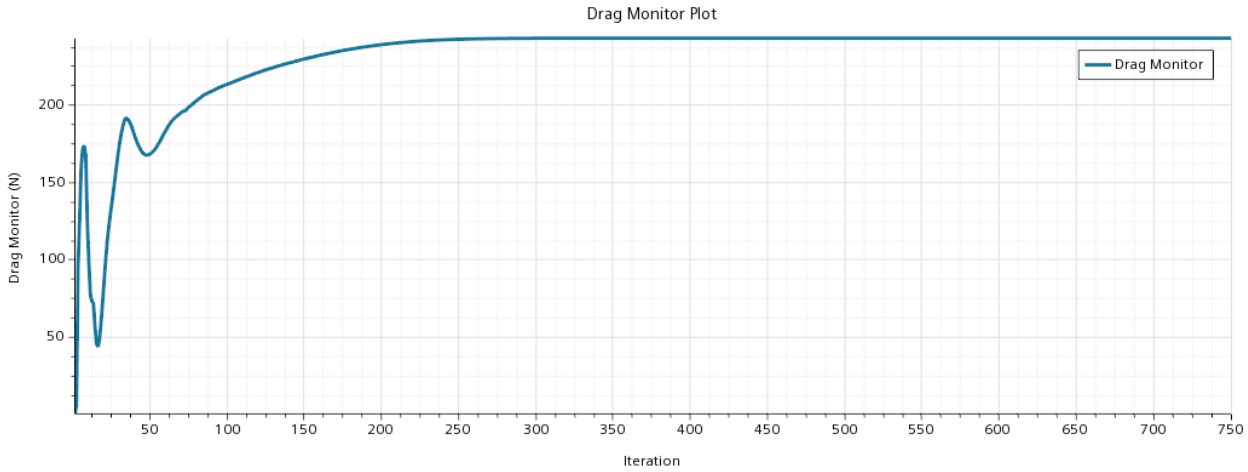

Figure 15: Drag monitor plot

5.3 Mesh Independence

Another factor to take into consideration is the mesh. For performing a proper study, the mesh must be independent, this means, must not affect the results obtained, being the cell size small enough to achieve this goal but not too small, since this would mean an unnecessary increase in the computational cost. In conclusion, the mesh must accomplish a satisfactory trade-off between accuracy of the results and the computational cost.

For achieving the mesh independence, three different cell sizes have been studied, comparing the results obtained for the three scenarios for drag and lift. Each mesh's cell size has been selected in order to increase in a 50% the number of cells in each one of the three directions. The criteria followed to classify a mesh as independent is having an error of under 5% (in both lift and drag) than the next smaller mesh.

The different mesh's sizes which have been used can be seen in Table 3, where "Main" and "Secondary" refer to the main or secondary wings' main chord.

	Mesh 1	Mesh 2	Mesh 3
Bullet shaped	65 Main	19.2 Main	5.7 Main
Foil Envelope	55 Main	16 Main	4.83 Main
Main Wing	45 Main	13 Main	3.95 Main
Wake Box 1	35 Main	10 Main	3.07 Main
Wake Box 2	35 Secondary	10 Secondary	3.07 Secondary

Table 3: Sizes of the different meshes in percentage of the different wings' main chord

After performing the required simulations the results found can be seen in Table 4.

	Mesh 1	Mesh 2	Mesh 3	Error 2-1	Error 3-2
Lift [N]	860.0081	942.2948	928.9199	9.87 %	1.42 %
Drag [N]	367.7094	251.8890	243.5742	45.98 %	3.41 %

Table 4: Relative errors in % for the different meshes

Plotting these results, a more visual representation of the mesh independence study can be seen in Figure 16 and Figure 17.

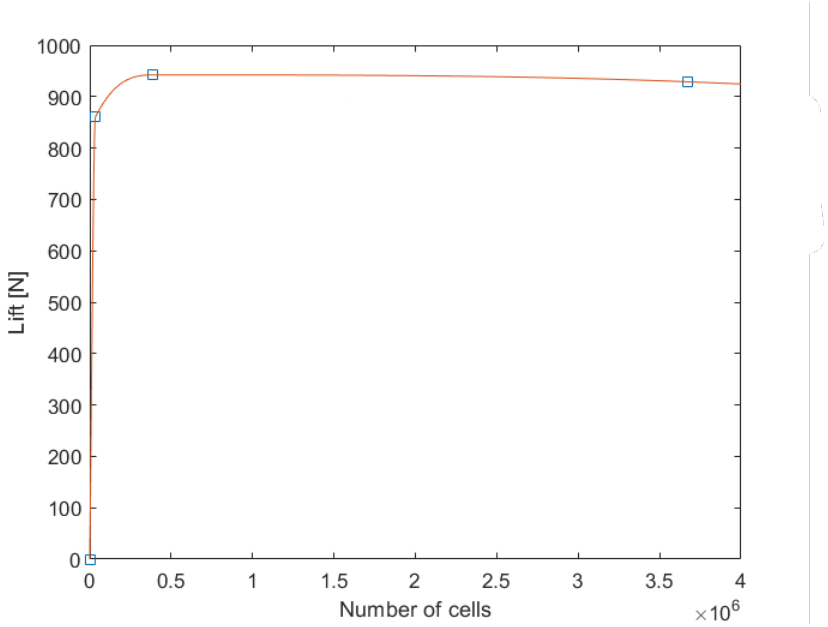

Figure 16: Lift calculated for each mesh

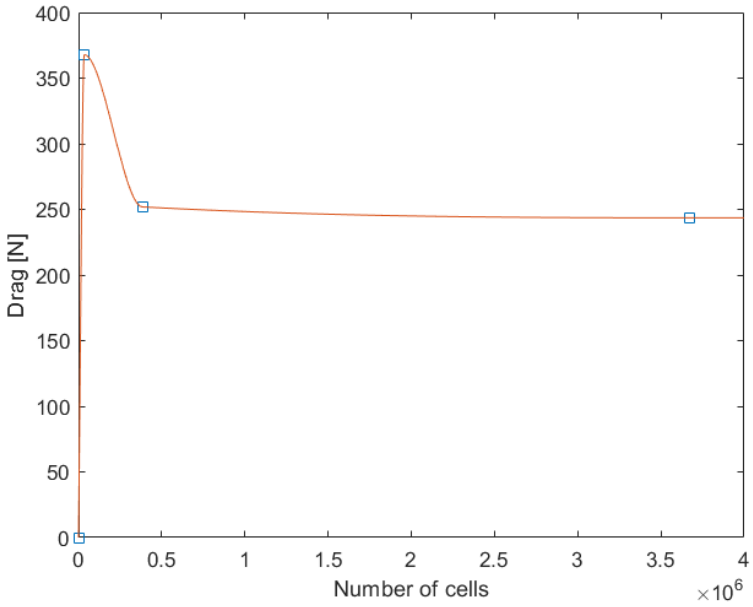

Figure 17: Drag calculated for each mesh

Seeing the results summarized in Table 4 , it can be concluded that the so called "Mesh 2" is independent, so those values of cell size will be used for every mesh needed along the study.

Focusing in the selected mesh, the cell distribution can be seen in Figure 18, Figure 19 and Figure 20

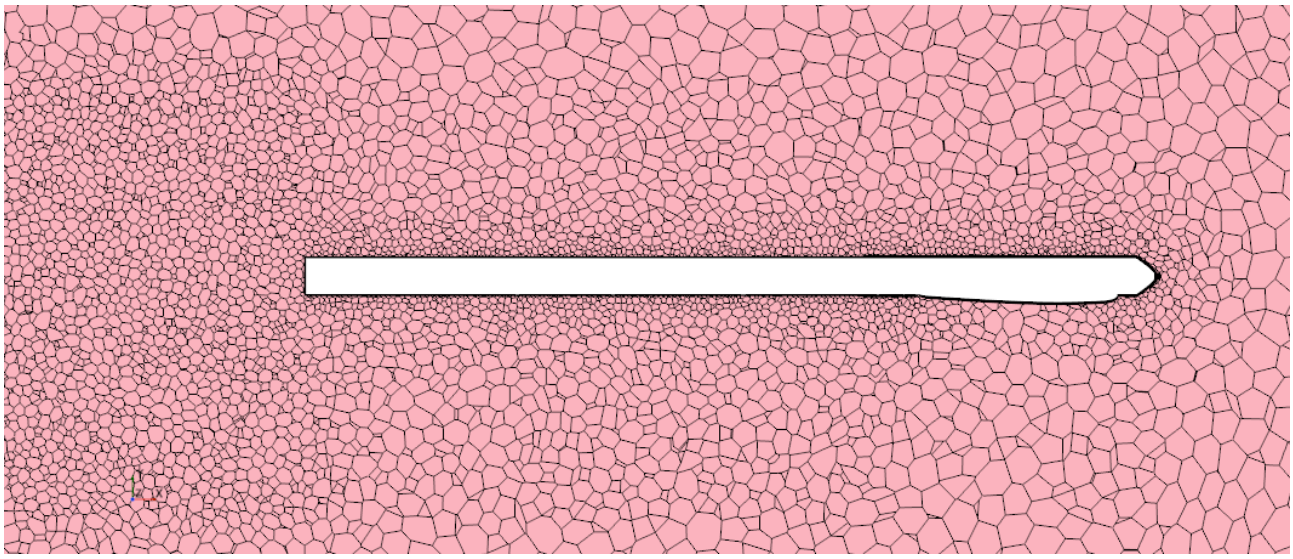

Figure 18: Selected mesh section

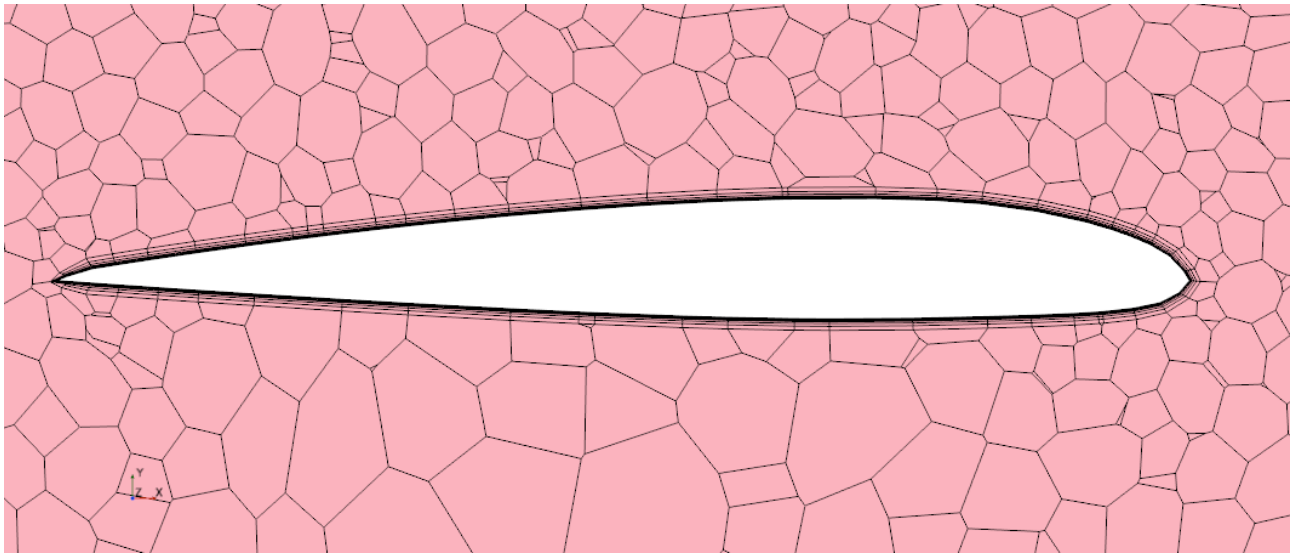

Figure 19: Selected mesh close up to main wing

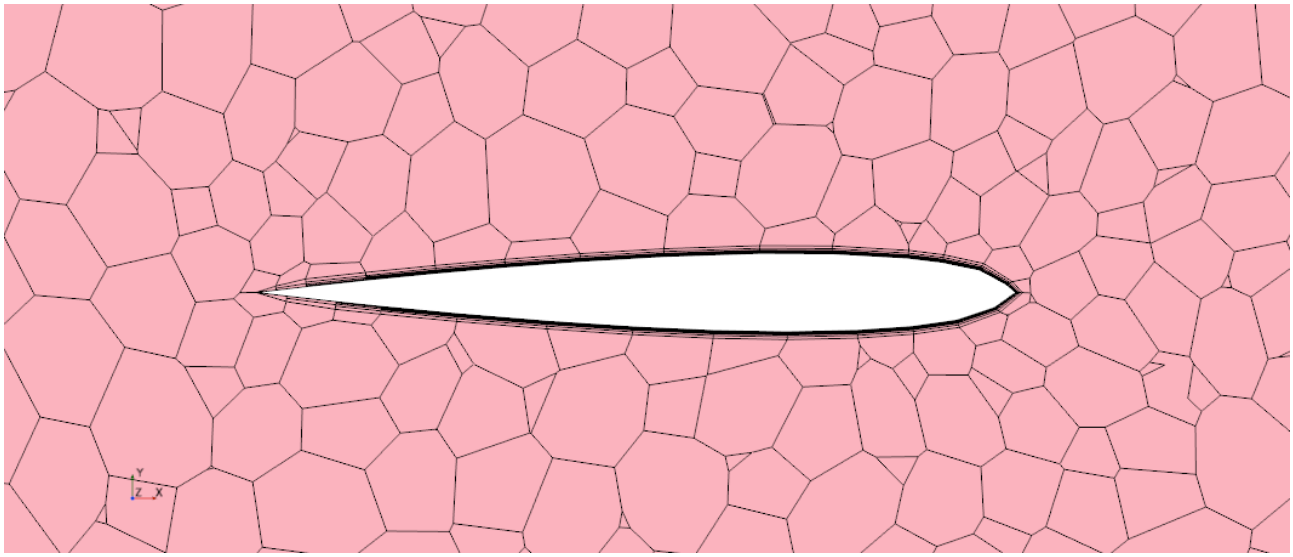

Figure 20: Selected mesh close up to secondary wing

As it can be seen, the cells' size adapts to the different volumes and values given and the prism layer is created smoothly around the bodies at the desired thickness stated before emulating the boundary layer. This will ensure a more accurate and realistic result when performing the simulations.

6 Results

Along this chapter the final designs will be presented analyzing their geometries and performances studied by performing different computational fluid dynamics simulations.

Before analyzing the designs themselves, it is important to understand the role and the different actions a pilot can do in order to control the prototype. The relative velocity needed respect to the water will be obtained by the tides and waves and, in a larger manner, by the wind. The user can control the speed transmitted considering two important factors, the wind's speed and the kite's size. The other method of control is changing its weight distribution, by balancing him or herself, the pilot can create or counteract the pitching moment generated by the hydrofoil, used to perform jumps or different acrobatics. The magnitude of the pitching moment generated by the hydrofoil will increase or decrease the difficulty of performing such acrobatics. Moreover, this weight balance can create rolling moments used by the pilot to perform turns.

Another key factor when designing hydrofoils for kitefoiling and when practicing the sport is to avoid cavitation. Cavitation occurs when the water vaporizes due to the lower pressure generated, in this case, since the hydrofoil is designed in order to obtain a pressure difference (to generate a lifting force) it may happen that the zone which generates the lower pressure produces a cavitation zone (if the pressure is lower than the seawater's vapor pressure [6]). Once cavitation occurs, the performance of the hydrofoil drops (the geometries are designed in order to perform underwater, once the fluid is changed to air, the design is not optimized) so the designer has to increase the cavitation velocity and study the cavitation velocity in order to know the hydrofoil's performance limit.

The first factor to study when analyzing the geometries will be the mesh quality, once this study has been performed, the results can be analyzed. The procedure followed for analyzing the results will consist in different steps. First of all, a sweep of lift, drag and pitching moment at different velocities will be performed in order to obtain the cavitation speed and a relation between the velocity and these factors, the next step will be to extrapolate from the relation obtained the velocity needed to lift an equivalent mass of 70 kilos, chosen as a reference pilot's mass. After this, a more in depth analysis of the flow behaviour will be done for the velocity calculated. This last analysis will be done in three different conditions, at zero degrees of angle of attack and roll and at the velocity needed to obtain the desired lift, at the that same speed and angle of attack but at $15^{\underline{o}}$ of roll, and at the minimum speed possible to obtain the desired lift by increasing the angle of attack.

6.1 Beginners' Design

This design is aimed at beginners, so its main objective is to allow the pilot to practice this sport in the easiest way possible. In order to obtain this, different key points must be considered:

- High pitching stability: an inexperienced pilot will not be able to balance his or her weight, so the pitching moment generated by the hydrofoil itself should be small enough to be easily controlled

- High rolling and yawing stability: for the same reason presented previously, the prototype should present null rolling and yawing moments generated and a resistance to external moments

imposed. Although this would make it harder to turn, it will avoid unexpected or unwanted turns due to pilot's unbalances.

- High lift coefficient: an inexperienced pilot should not travel at higher velocities due to the risks this mean, so he or she should be able to enjoy the sport and gain experience by travelling at lower speeds. This means the hydrofoil used will need to generate enough lift at lower speeds.

Once the list of requirements is done, it is possible to design an appropriate geometry.

6.1.1 Geometry's Description

Attending to the previously exposed requirements the design developed can be seen in Figure 21 and is explained below.

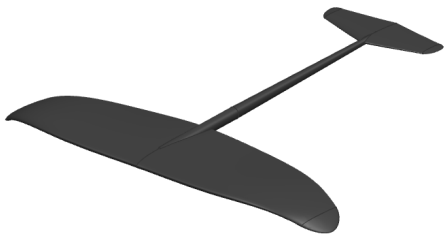

Figure 21: Beginners' design perspective view

Analyzing the geometry in detail, there are some aspects to comment. As it can be better seen in Figure 22, obviously, the design is completely symmetric in its longitudinal axis, this feature will satisfy the requirement of a null rolling and yawing moments generated by the geometry itself.

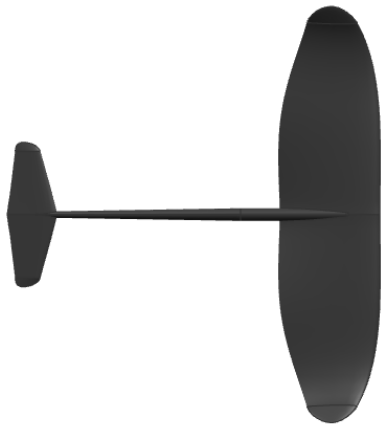

Figure 22: Beginners' design top view

Another important feature are both wing's wingtips design, easily seen in Figure 23 and Figure 24. Both, the secondary and main wing's wingtip is designed to create an elliptical wing, this is done in order to reduce the induced drag, increasing the efficiency of the geometry, although reducing the drag is not an explicit requirement, increasing its efficiency is a general requirement in any design. Moreover, the main wing's wingtip is curved downwards at an angle of 30^{o}, this is done in order to increase the lateral area of the wing, thus increasing the drag presented when a lateral displacement is performed, increasing the design stability .

Figure 23: Beginners' design front view

Figure 24: Beginners' design side view

The pitching stability requirement is fulfilled thanks to the secondary wing, which has a symmetric profile. This allows the wing to perform properly in a wider range of angles of attack, both positive and negative, always in a stabilizing manner, this is, a perturbation which induces angle of attack will generate a force tending to reduce that angle to zero. Also, a small pitch is needed to compensate the slight weight the pilot can place in her or his front foot.

The geometry main characteristics are summarized in Table 5.

Main wing	
Profile	NACA1012
Maximum thickness	25 mm
Span	820 mm
Aspect ratio	9.05
Secondary wing	
Profile	NACA0012
Maximum thickness	12 mm
Span	280 mm
Aspect ratio	8.01
Fuselage	
Length	610 mm

Table 5: Beginners' geometry main characteristics

The secondary wing is symmetric in the whole span but the main wing has a more complex geometry. It has a symmetric profile NACA0012 [7] for the first 40 mm from the symmetry plane in each direction and then evolves until reaching the main profile mentioned in Table 5 at 165 mm from the symmetry plane. From that point, the chord starts decreasing and at 290 mm from the symmetry plane starts the downwards deviation of the wingtip easily seen in Figure 23. The distances between the symmetry plane and the main profile have been selected in order to minimize the fuselage interferences, since a more cambered profile will be less adaptable to the impact the fuselage has on the flow. For the fuselage, it is a cylinder which extends between the points of maximum thickness of both wings and its thickness varies in order to adapts to each wing. Both fuselage's ends are rounded in a spherical way in order to reduce the drag generated by the fuselage.

6.1.2 Geometry's Analysis

As mentioned, before analyzing the results themselves it is important to check the mesh quality. With this purpose, in Figure 25 the mesh is shown from a side view. It can be seen that the cells adapt to the sizes specified previously in this document.

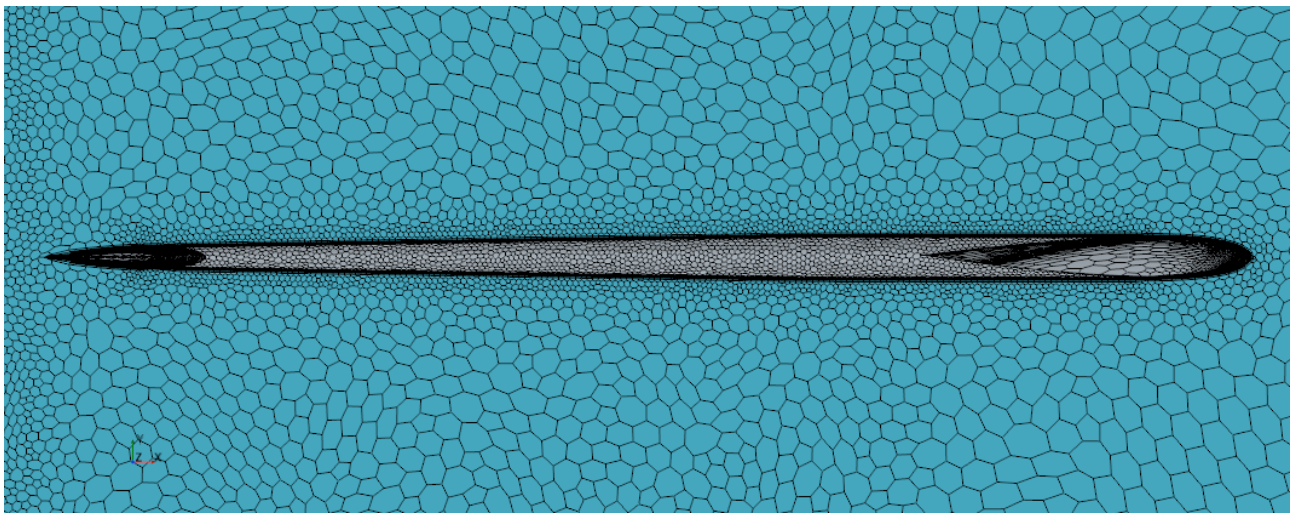

Figure 25: Beginners' design mesh generated side view

Is important to check not only the cells' size but also the prism layer quality. In Figure 26 and Figure 27 a front view of both of the wings including the wingtips, which are the most critical zone due to its small size are shown. As it can be seen, the mesh adapts to the different body sizes according to the parameters explained previously in this document.

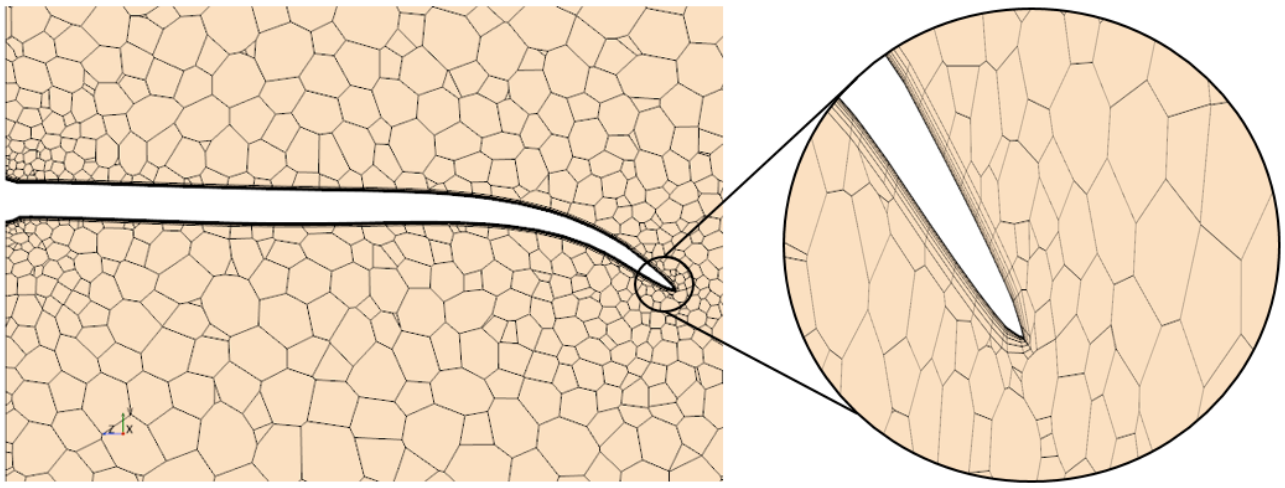

Figure 26: Beginners' design main wing mesh generated front view

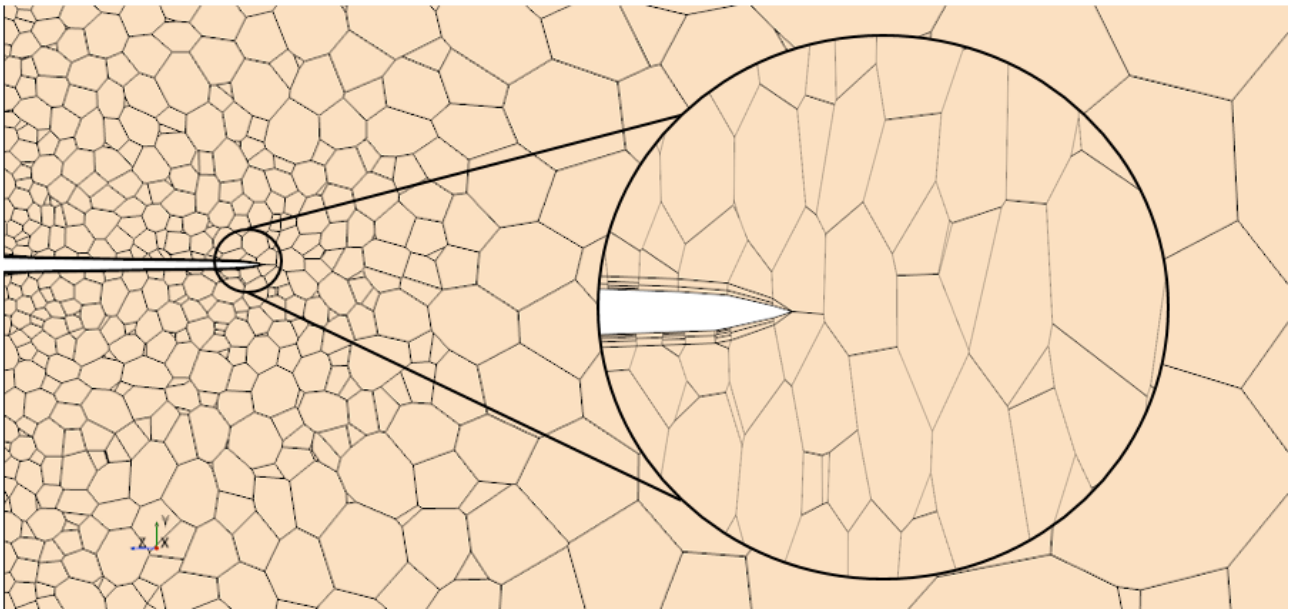

Figure 27: Beginners' design secondary wing mesh generated front view

Following the procedure established, the first analysis performed has been a velocity sweep at zero degrees of angle of attack in order to know the main forces (lift and drag) and moments (pitching) at different speeds and to obtain the last point before cavitation (recognised once the pressure at any point around the geometry drops below the seawater vapor pressure [6]). Note that, due to the nautical nature of the project, the velocity will be expressed in knots for this first analysis. Moreover, in order to give the information in a more user-friendly way and to adapt the information to the format used in the industry, the data shown in Figure 28 will be the mass equivalent to the lift generated as expressed in the formula seen in Equation 1, where "L" is the lift force and "g" is the gravity's acceleration at the Earth.

$$M_{eq} = L/g \tag{1}$$

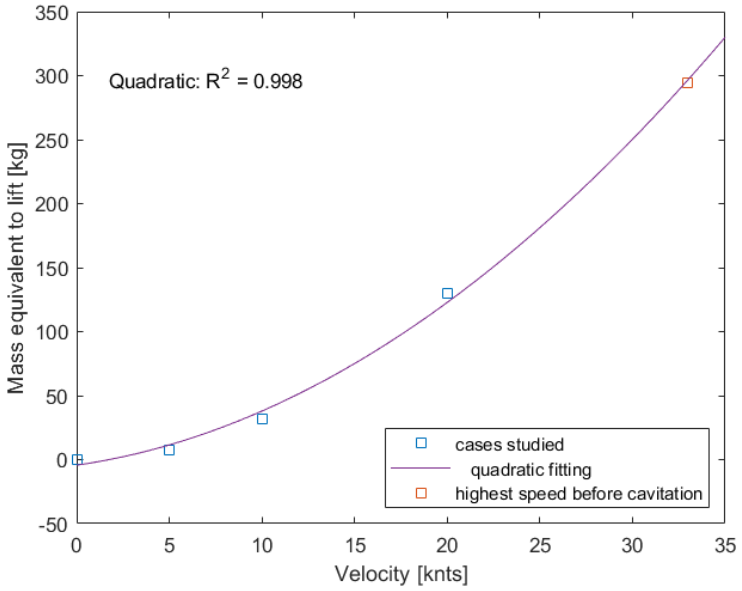

Figure 28: Mass equivalent to lift generated at different velocities for beginners' design

The results seen in Figure 28 show the fulfillment of the third requirement established (high lift coefficient), since, considering the wind velocities at coast zones [8], a high enough velocity to lift up a pilot is easily achievable at most of the coastal areas.

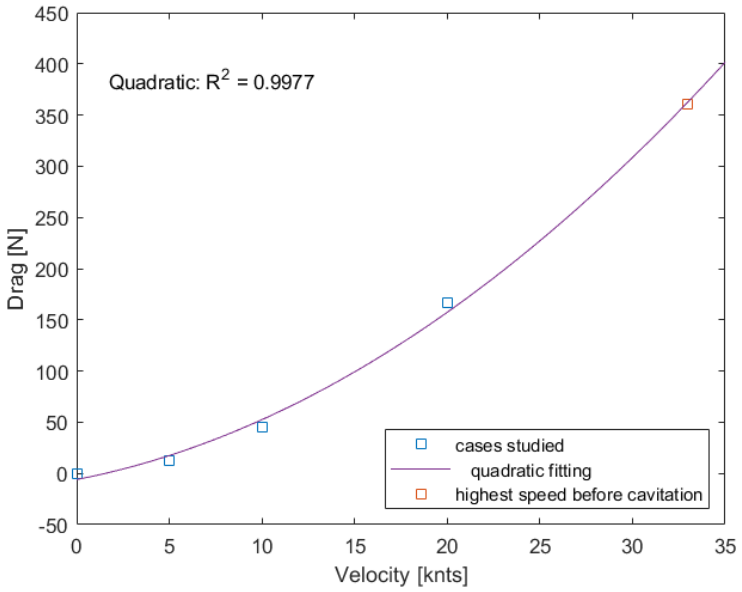

Figure 29: Drag generated at different velocities for beginners' design

From the data shown in Figure 28 and Figure 29 the efficiency of the geometry can be calculated by dividing the lift and the drag, obtaining, for a velocity high enough to lift the 70 kilos mentioned, a value of 7.05.

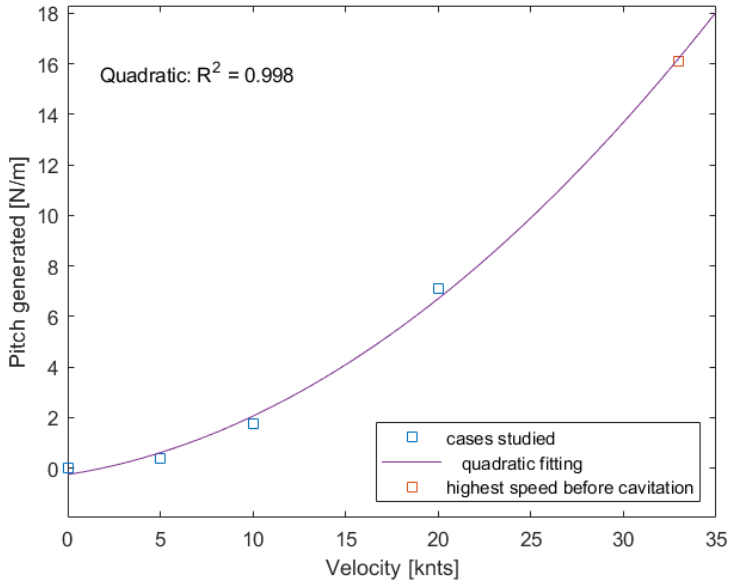

Figure 30: Pitching moment generated at different velocities for beginners' design

The data shown in Figure 30 shows the fulfillment of the first requirement (high pitching stability). The pitching moment is not zero but is low enough to be easily controlled by the pilot, also is high enough to compensate the moment generated by the weight distribution of the pilot. Note that, for the whole project, a positive pitching moment means a nose up movement.

As expected, in all three analysis the results follow a quadratic expression with a high precision. It can also be seen that the limitations in speed due to cavitation are at 33 knots (or 16.98 meters per second), for higher velocities the water begins to cavitate due to the low pressure generated at the suction zone of the main wing.

Extrapolating from Figure 28 and selecting a mass of 70 kilos as an average user's mass, a velocity of 14.28 knots (or 7.34 ,eters per second) has been selected to perform further analysis, studying the flow behaviour around the geometry. For this purpose several flow properties have been studied. Note that, although when performing the simulations just half the body has been studied due to its symmetry, when post-processing, the results have been duplicated whenever possible taking into consideration that same symmetry plane.

Beginners' design analysis: 14.28 knots no angle of attack no roll

Starting with the study of the vorticity seen in Figure 31 and in Figure 32, it can be seen that the wake generated by the design is mainly due to the fuselage and not the wings, validating the wingtips functionality since their main objective is to reduce the wake generated in order to reduce the induced drag.

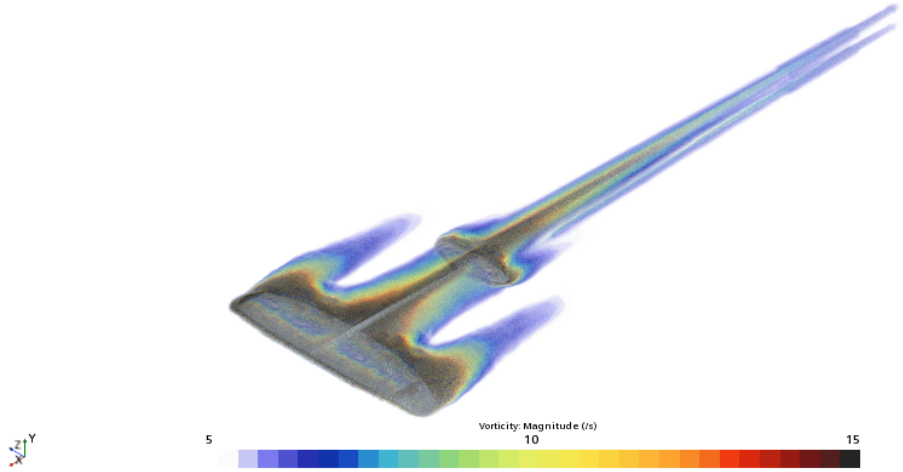

Figure 31: Beginners' design vorticity contour

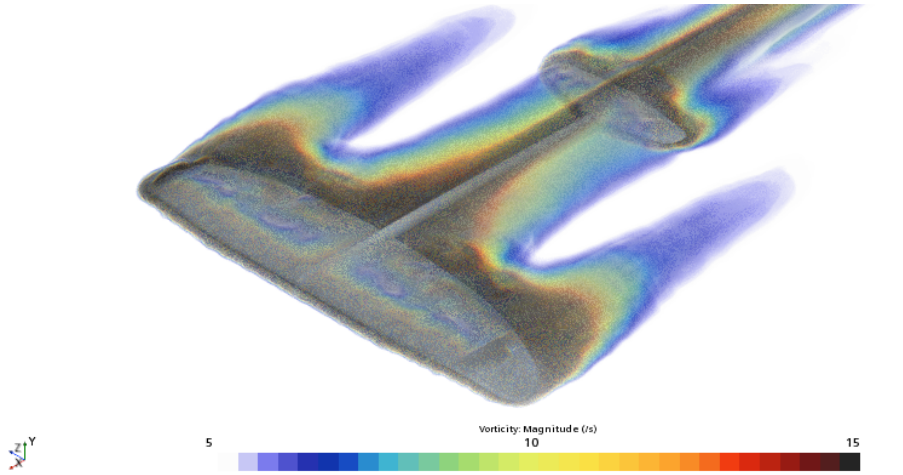

Figure 32: Beginners' design vorticity contour close up to the geometry

The next step in the analysis will be studying the velocity and trajectory of the flow at different planes and from different points of view.

Starting from the front view of the main wing, in Figure 33 the wingtips performance can also be studied. The colours of the contour indicate the velocity magnitude while the lines show the flow's trajectory. As it can be seen and as expected, there are still wingtip vortexes although elliptical wings have been used but this wingtips cause that those zones are of a smaller magnitude. The colours seen above the wing indicate a higher speed at the top part of the wing, this is equivalent to a suction zone, while at the bottom part it can be seen a slower velocity, equivalent to a higher pressure. This pressure difference between top and bottom is the cause of the lift generated.

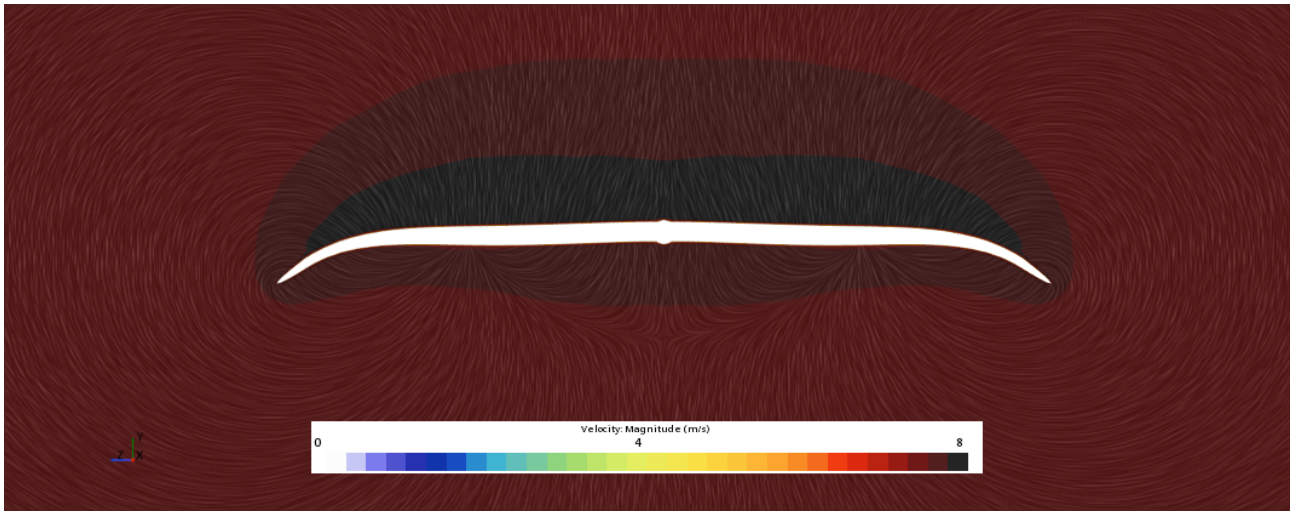

Figure 33: Beginners' design main wing front view velocity contour

Switching the focus to the secondary wing, in Figure 34 it can be seen how the main wing's wingtip vortexes are extended until the secondary wing as seen in Figure 31, this will be the cause of the smaller velocity zones seen at the sides of the secondary wing, since the main wing's wingtip vortexes collide with the secondary wing's ones creating these zones. Moreover, it can also be seen a similar behaviour regarding the trajectory, only varying the amplitude of the wingtip vortexes, being smaller in this case. This is due to the geometry of the wing itself, since it is smaller and has a symmetric profile, it should generate no lift, so the difference in velocity and pressure between both sides of the wing are smaller causing wingtip vortexes of a smaller magnitude. Also the magnitude of the velocity is not apparently higher in the top or the bottom of the wing (the colours are pretty similar above and under the geometry), this is once more due to the wing's profile, a symmetric profile without angle of attack will not generate a different velocity in each side. In this case, although the real angle of attack is not zero but the one induced by the downwash of the main wing, this angle is very small.

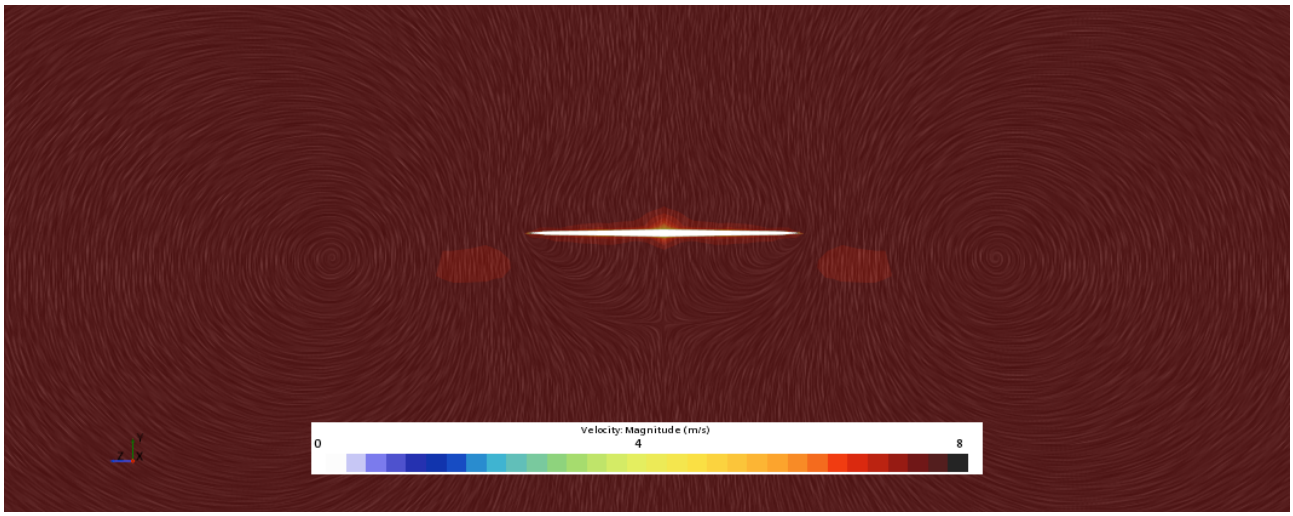

Figure 34: Beginners' design secondary wing front view velocity contour

In Figure 35 and Figure 36, it can be seen that there is no difference in pressure coefficient

along either the chord or the span, validating the point established before about the lack of pressure difference between bottom and top of the secondary wing in a more precise way. Just a small difference at the leading edge can be seen in Figure 35, caused by the small negative angle of attack induced by the main wing's downwash and generating the small downwards force which will generate the pitching moment calculated in Figure 30.

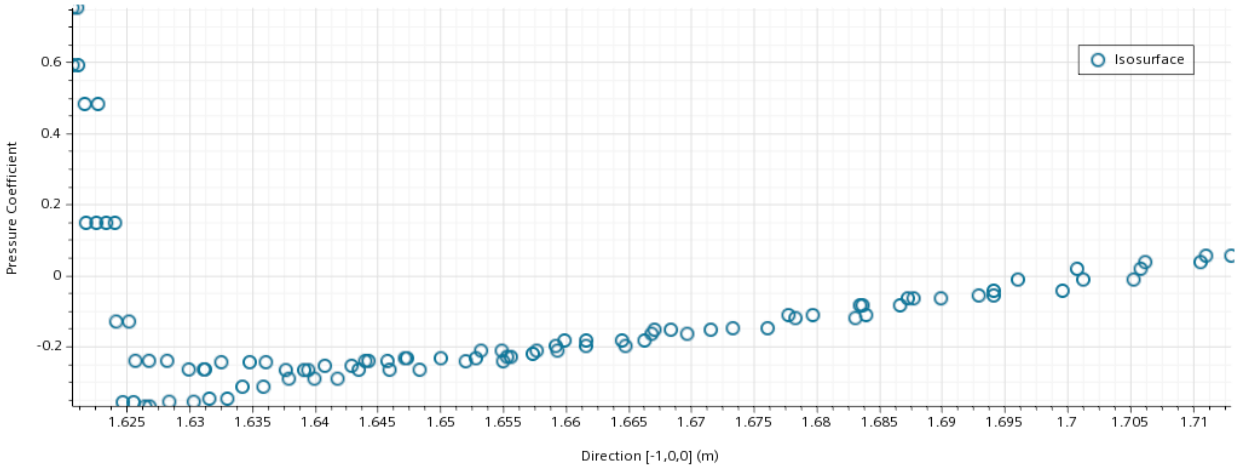

Figure 35: Beginners' design secondary wing pressure coefficient distribution along the chord

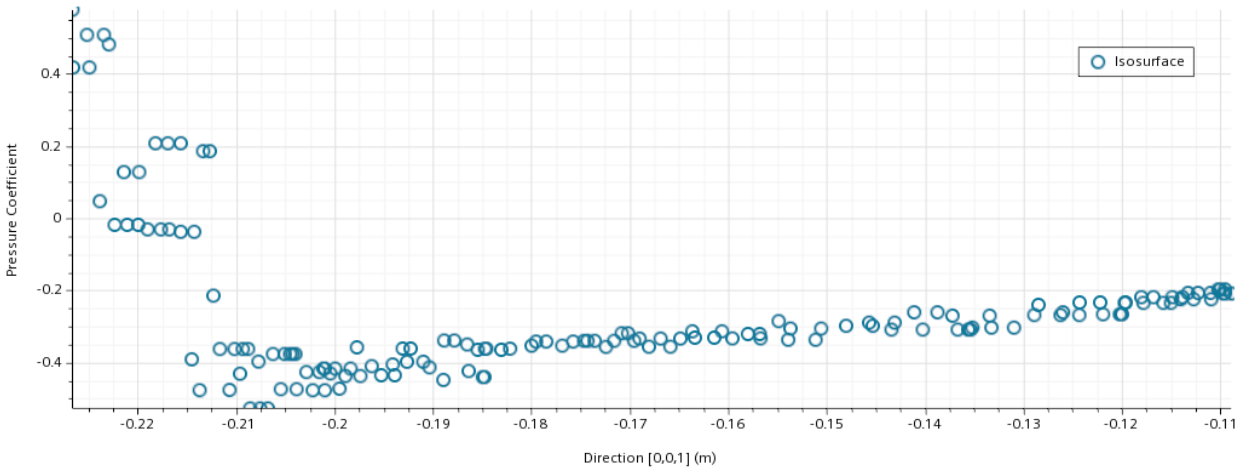

Figure 36: Beginners' design secondary wing pressure coefficient distribution along the span

By varying the section studied until the point where the flow has already traversed the whole geometry the wake generated can be seen in Figure 37 as the zone of low velocity. As expected (based in results seen in Figure 31) the fuselage is the responsible of most part of the wake, this is due to two main reasons, the fuselage's length, since the flow loses its energy by the friction with the body, the longer the body the higher the amount of energy lost, and the fuselage's end shape, which, since is a half sphere, may be perceived by the fluid as an abrupt change. It can also be seen how this effect decreases as the distance to the fuselage increases.

In Figure 37 it can also be seen how the both of the wing's wingtip vortexes are extended downstream.

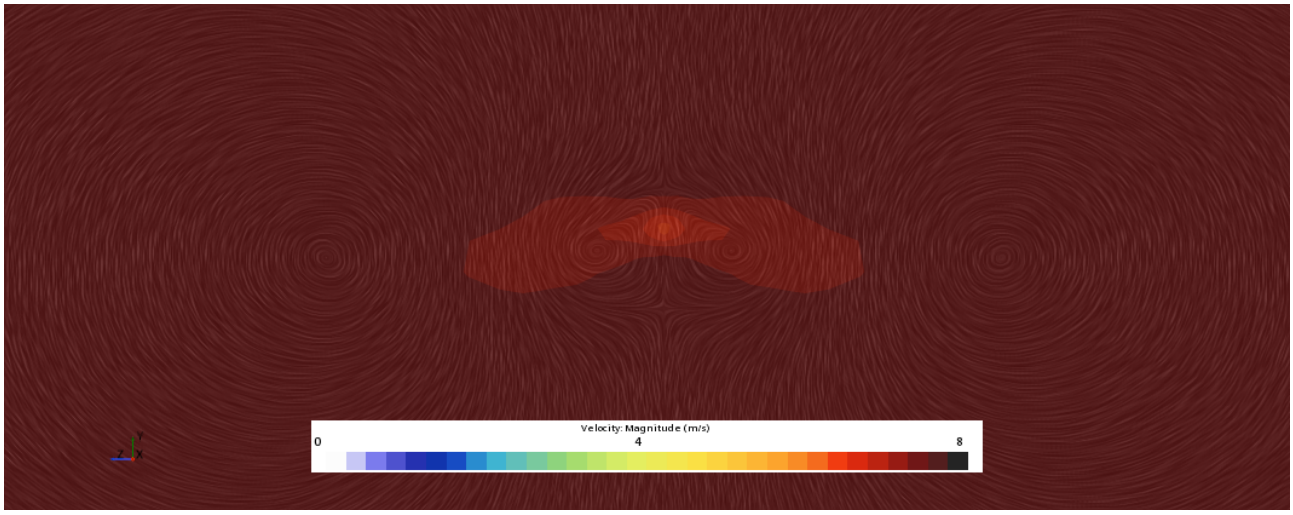

Figure 37: Beginners' design wake front view velocity contour

Now switching to a side point of view, the wake can be still studied. In Figure 38 it can be seen how the fuselage creates a zone where the velocity is reduced significantly due to the loss of energy of the flow. This loss of energy begins to be noticeable at the last parts of the fuselage where the boundary layer begins to increase its thickness. It can also be seen how the interaction between the main wing's leading edge and the fuselage front already generates a zone of higher velocity above the main wing. Once the main wing chord is already passed by the flow, this zone does not appear since the symmetric fuselage dos not generate a difference in velocities itself.

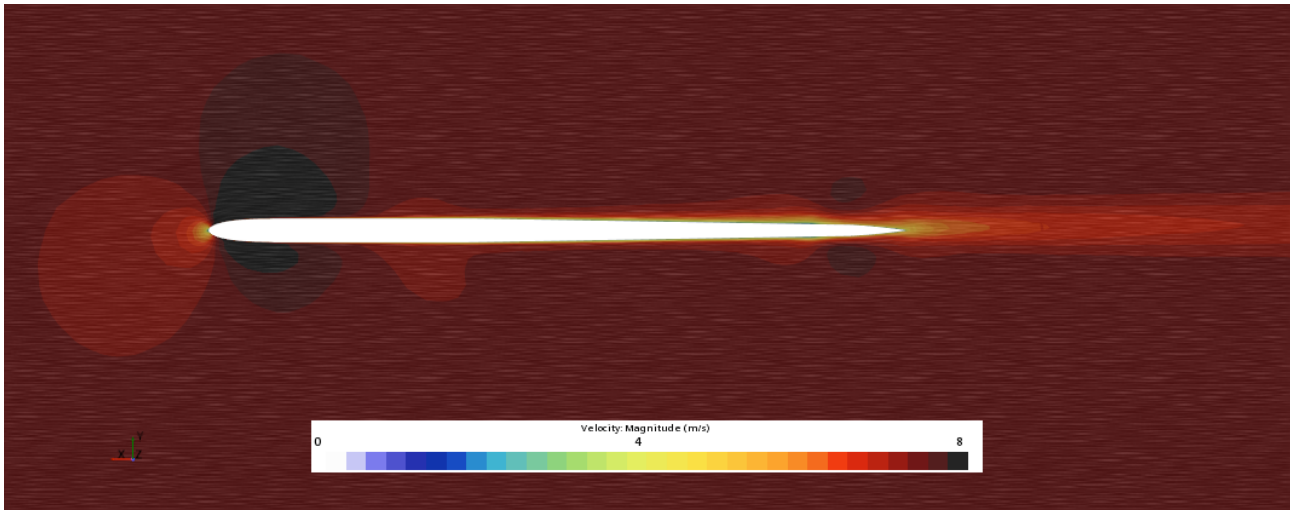

Figure 38: Beginners' design symmetry plane velocity scene

Varying the section studied, the magnitude of the mentioned downwash of the main wing can be studied in Figure 39. It can be seen how the trajectory of the flow is not significantly different before and after the main wing affects it, confirming that the induced angle of attack to

the secondary wing is approximately zero but not zero, this is appreciated due to the fact that from this point of view a difference in the velocity contours above and under the secondary wing is appreciated, causing, in this case, a downwards force since the higher velocity, and therefore the lower pressure, is located under the wing. This is due to the fact that the downwash of the main wing generates a displacement in the stagnation point of the secondary wing, creating a negative angle of attack. This downwards force created by the secondary wing will be the cause of the pitching moment seen in Figure 30.

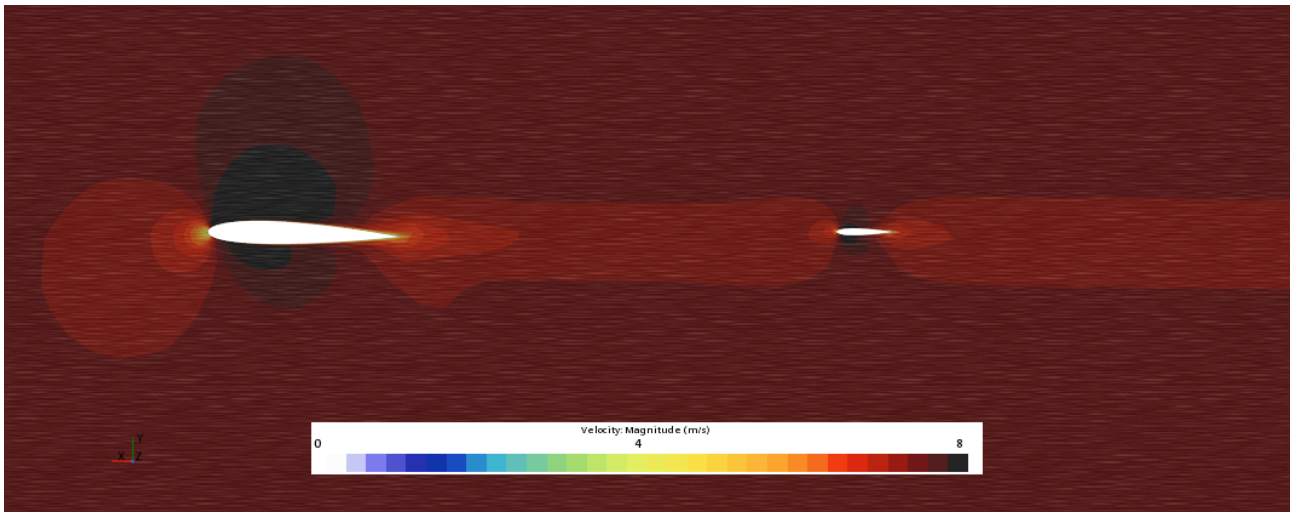

Figure 39: Beginners' design side view velocity scene

Beginners' design analysis of roll angle

Now the next scenario analyzed as stated before will be a roll angle of 15^{o} at 0^{o} of angle of attack without varying the velocity, simulating a right turn performed by the pilot. Note that in this case the symmetry plane is lost due to the roll so the whole geometry has to be simulated. The main forces and the pitching moment generated can be seen in Table 6. Due to roll, the hydrodynamic force is now divided into three components: vertical upwards, lateral force and drag. The upwards component is used to keep the pilot lifted, and the lateral force is used to perform the turn.

Lateral force	Upwards force	Drag	Pitching moment
165.27 [N]	616.61 [N]	88.43 [N]	5.69 [N/m]

Table 6: Beginners' geometry at 15^{o} of roll main forces and moment

Starting by the vorticty contour, seen in this case from a top point of view in order to avoid misunderstanding the contour created because of the perspective, in Figure 40 it can be seen how the roll does affect the wake symmetry but does not affect the wingtips' performance. In this case, the wake generated by the lowered half wing, seen in the left side of the image, is wider than the generated in the other half wing, this is due to the lateral component of the flow induced by the roll angle.

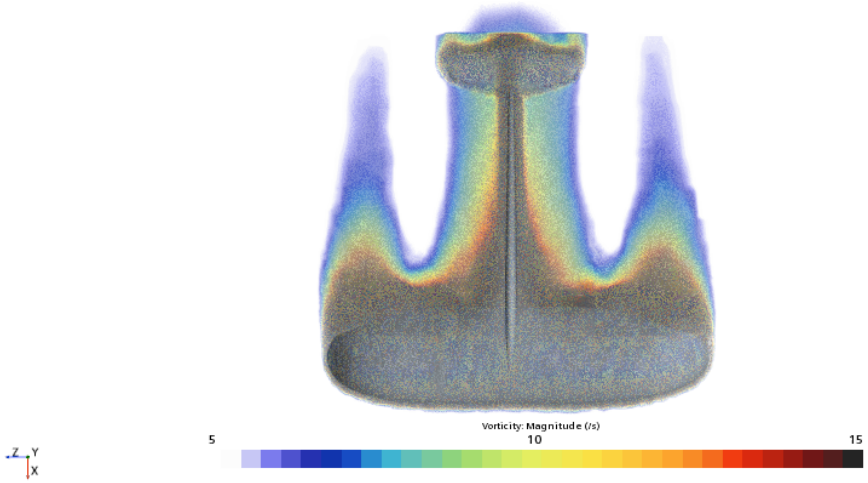

Figure 40: Beginners' design vorticity contour at 15º of roll

As seen in Figure 41 and Figure 42 for the main wing the suction zone is still generated in the upper part of the main wing while in the secondary wing, although the angle of attack is zero and is symmetric, the downwash from the main wing creates an equivalent angle of attack, generating a zone of lower velocity (higher pressure) at the upper part of the wing, this will be the cause of the pitching moment generated. It can also be seen how the both wing's wingtip vortexes are generated and extend downstream. This vortexes are the cause of the lower velocity zones seen in Figure 42 since they rotate in different directions so, when they collide this lower velocity zones can be seen.

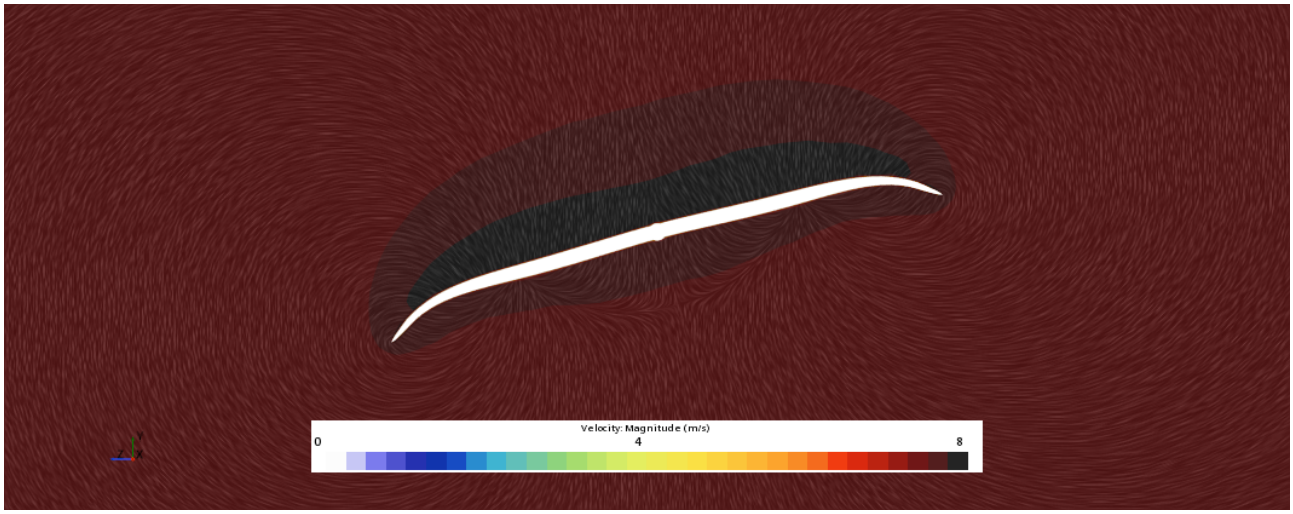

Figure 41: Beginners' design main wing front view velocity contour at 15º of roll

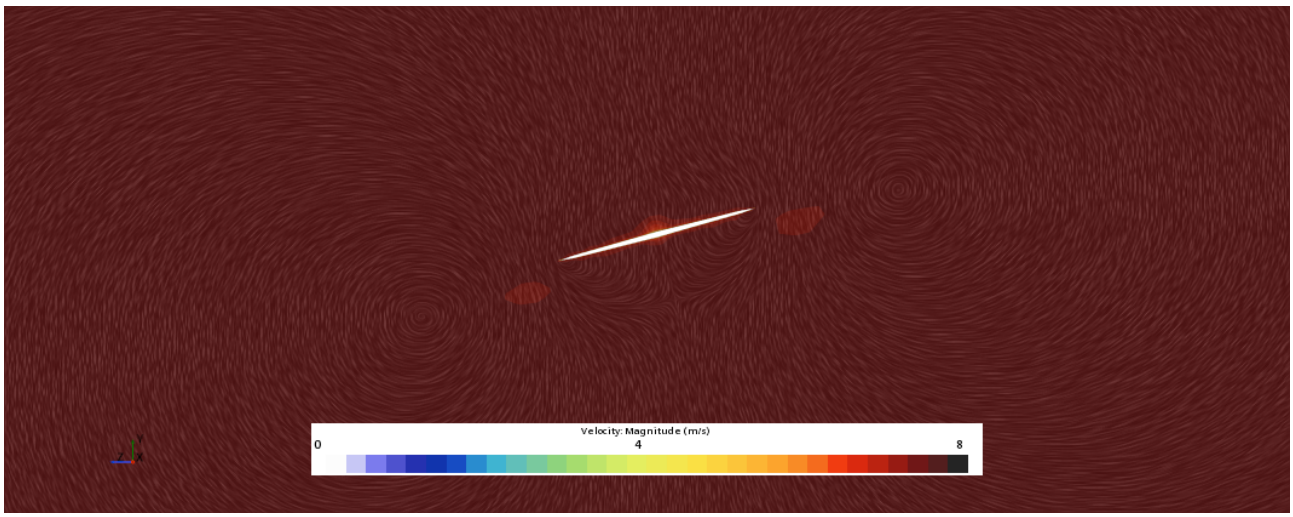

Figure 42: Beginners' design secondary wing front view velocity contour at 15º of roll

When analyzing the wake generated, in Figure 43 it can still be seen how the main recirculation zone appears behind the fuselage, where the velocity is lower, as expected from the results seen in Figure 40.

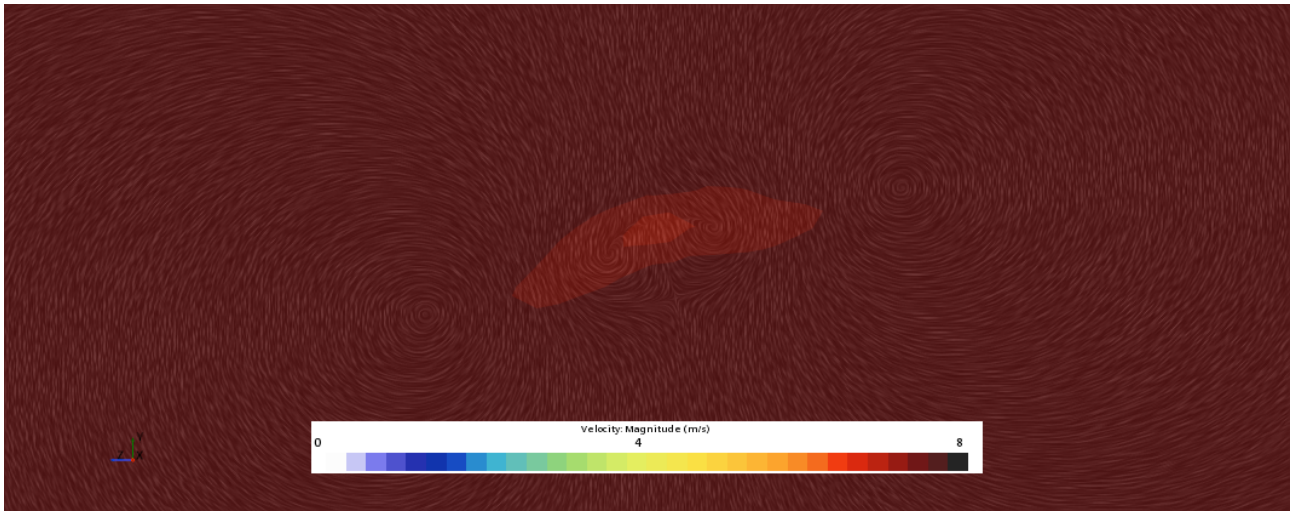

Figure 43: Beginners' design wake front view velocity contour at 15º of roll

Switching to a side point of view, the asymmetry seen before is maintained, as seen in Figure 44 and Figure 45, the roll movement generates a zone of higher velocity on the upper part of the main wing. The stagnation point is similar in both sections.

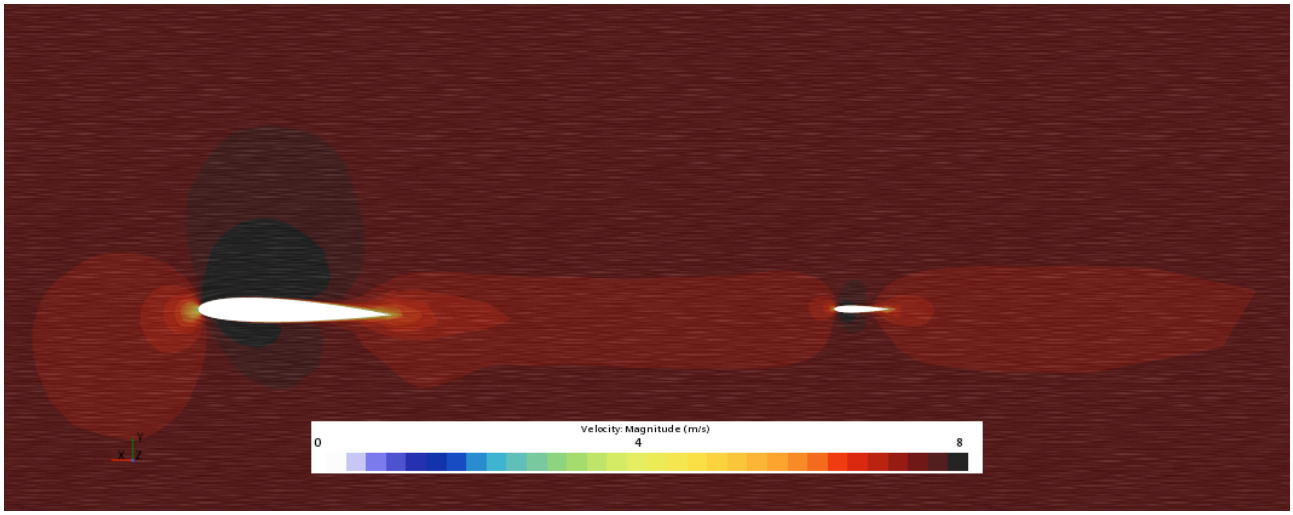

Figure 44: Beginners' design right side view velocity contour at 15º of roll

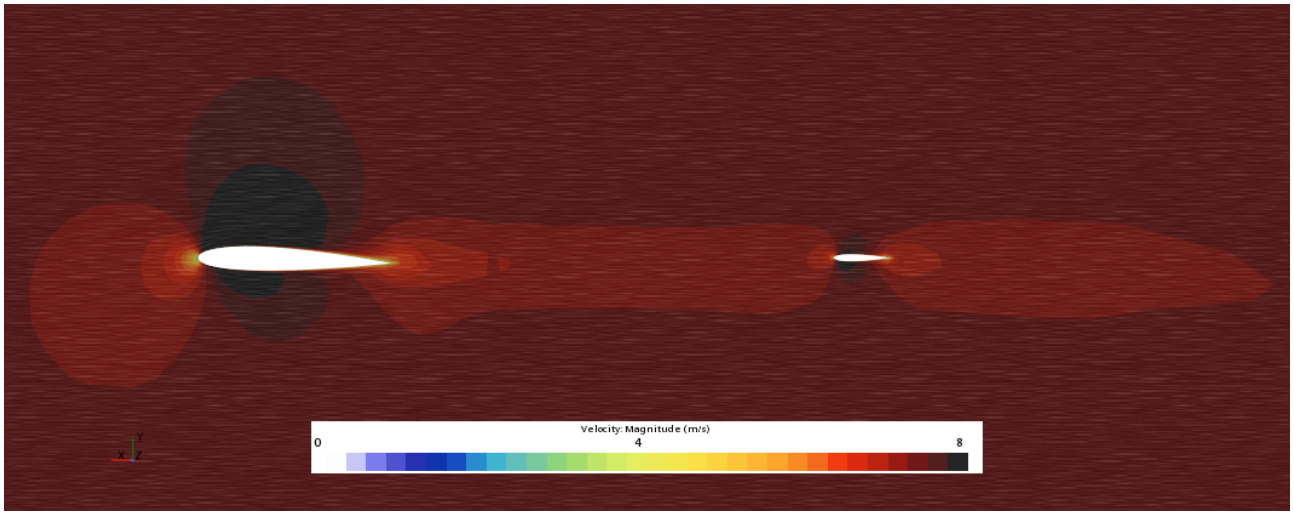

Figure 45: Beginners' design left side view velocity contour at 15º of roll

For the middle of the geometry, as seen in Figure 46, the main effects of the roll are seen in the wakes generated.

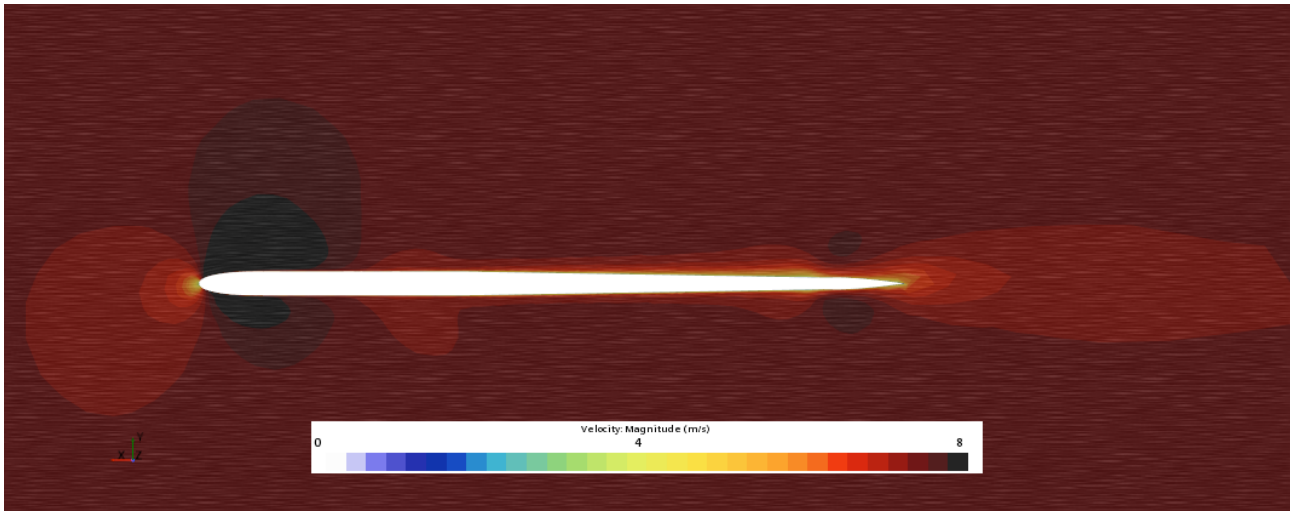

Figure 46: Beginners' design symmetry plane side view velocity contour at 15^{o} of roll

Beginners' design analysis of angle of attack effect

The last step of the analysis is to come back to a roll angle of 0^{o} and to increase the angle of attack in order to reduce the velocity needed to reach the lift required to lift the 70 kilos specified previously. It is important to consider that the angle of attack can not be increased as desired while the velocity is reduced drastically because it would mean the detachment of the boundary layer. For this reason, the angle of attack has to be gradually increased while reducing the velocity until a point where the boundary layer is not detached and the lift generated is increased.

For this geometry, this relation and the resultant forces and pitching moment are shown in Table 7.

Angle of attack	Velocity	Lift	Drag	Pitching moment	Efficiency
4 [^{o}]	9.33 [knts] = 4.8 [m/s]	753.62 [N]	67.46 [N]	-7.36 [N/m]	11.17 [-]

Table 7: Beginners' geometry angle of attack main forces and moment

The lift generated is increased when increasing the angle of attack for different reasons. First of all, now the whole wing is generating lift while the parts being symmetric near the fuselage were not generating lift at 0^{o} of angle of attack. Also, increasing the angle of attack varies the location of the stagnation point, creating a different distribution of pressures, generating a different resultant in the forces generated and moreover, now the secondary wing also generates lift.

By increasing the angle of attack, the speed needed to obtain the desired 70 kilos (approximately, since more force is actually generated) of mass equivalent to lift is reduced by about 5 knots. Also, it can be seen that the secondary wing accomplishes its stabilizing purpose since the pitch generated is negative, meaning it tends to create a nose down movement, changing the angle of attack to 0^{o}. Once the forces and moment have been calculated, the same analysis of the flow behaviour performed previously can be done. Starting with the vorticity analysis, in Figure 47 can be seen how the intensity of the vortexes generated is higher when the angle

of attack is increased. This is related with the lift increase. Although the intensity is increased, the wake generated does not increase significantly, thus increasing the total efficiency because the lift increases much more than the drag does since the wingtips still avoid the formation of relatively high intensity wingtip vortexes which would increase the induced drag generated. The scene also shows how the wake generated will still be focused around the fuselage and will be bigger in size but extend for a lower distance than the case with no angle of attack seen in Figure 31.

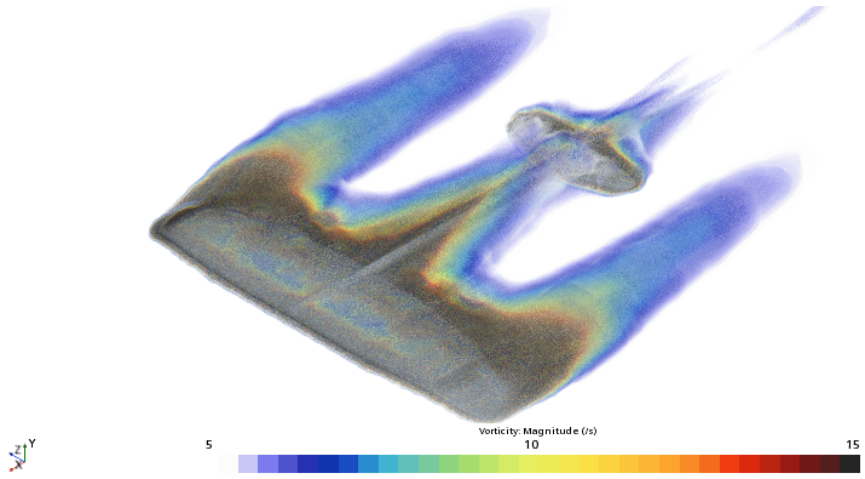

Figure 47: Beginners' design vorticity contour at 4º of angle of attack

Analyzing the main wing from a frontal point of view, it can be seen in Figure 48 how the velocities obtained in the upper part of the wing are higher since the angle of attack has increased, this mean a lower pressure thus a higher lift generation. Focusing in the lines that show the flow trajectory, it can be confirmed that the wingtips successfully achieve to avoid the creation of wingtip vortexes has mentioned before.

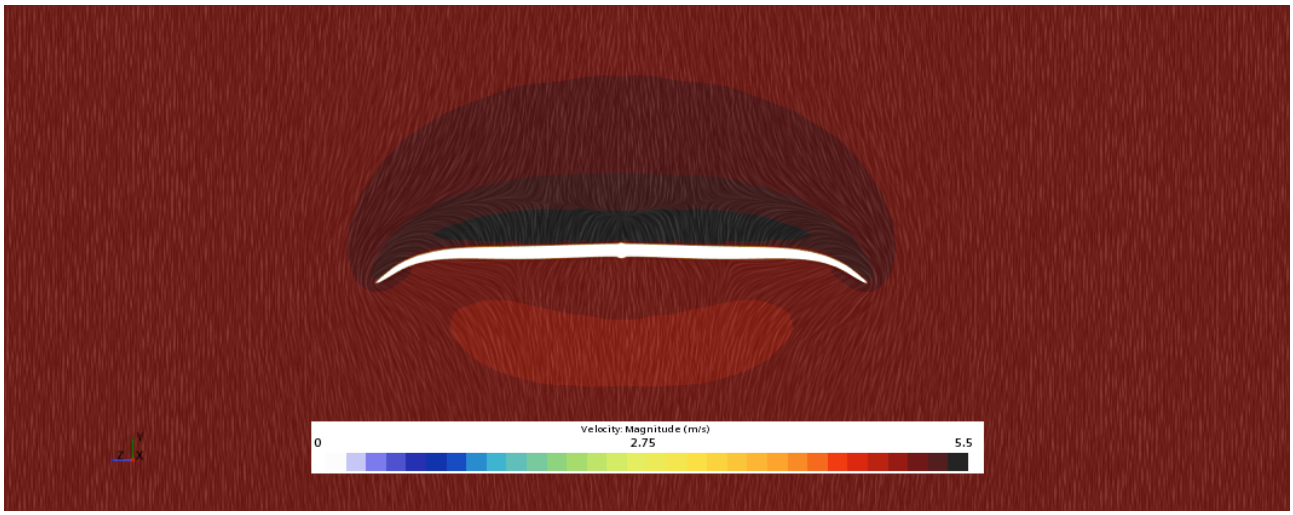

Figure 48: Beginners' design main wing's front view velocity contour at 4º of angle of attack

Switching the plane to the secondary wing, in this case the main wing's downwash will

still impact the secondary wing's performance but the increase in angle of attack will reduce its effect. In Figure 49 and Figure 50 it cannot be seen a significantly bigger suction zone in any of the sides of the secondary wing. A different contour will be seen in order to justify the lift generated by the secondary wing. Once again, it can be seen the formation of two lower velocity zones at the sides of the secondary wing, this is also due the collision of both of the wingtip vortexes generated in each wing.

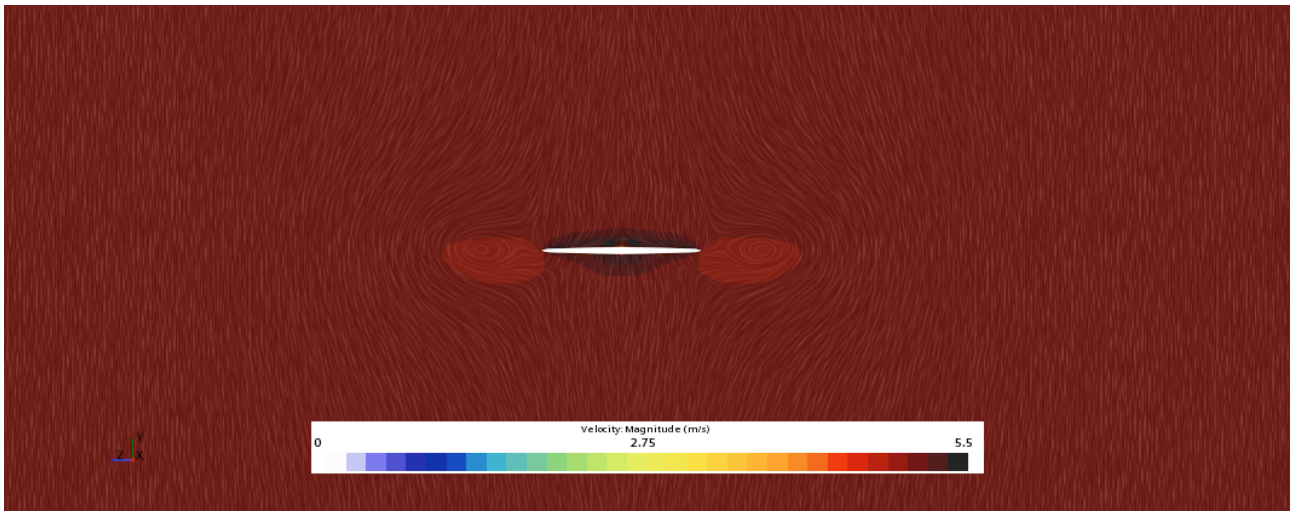

Figure 49: Beginners' design secondary wing's front view velocity contour at 4º of angle of attack

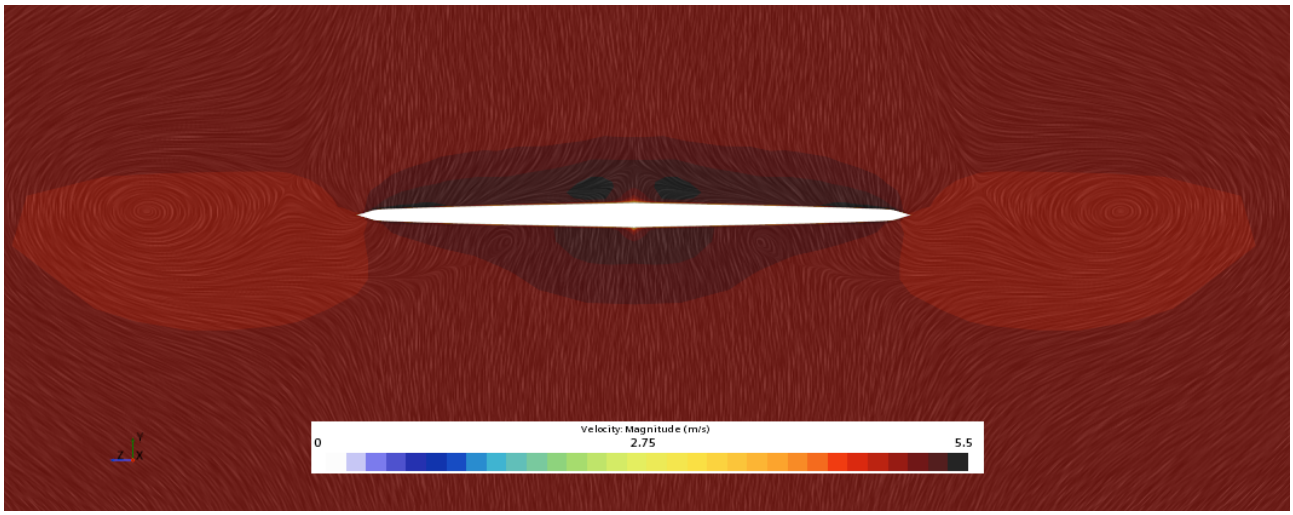

Figure 50: Beginners' design secondary wing's close up front view velocity contour at 4º of angle of attack

In Figure 51 and Figure 52 it can be seen how there is a pressure difference between the top and the bottom parts of the secondary wing, reinforcing the comment above and justifying the negative pitching moment calculated in Table 7.

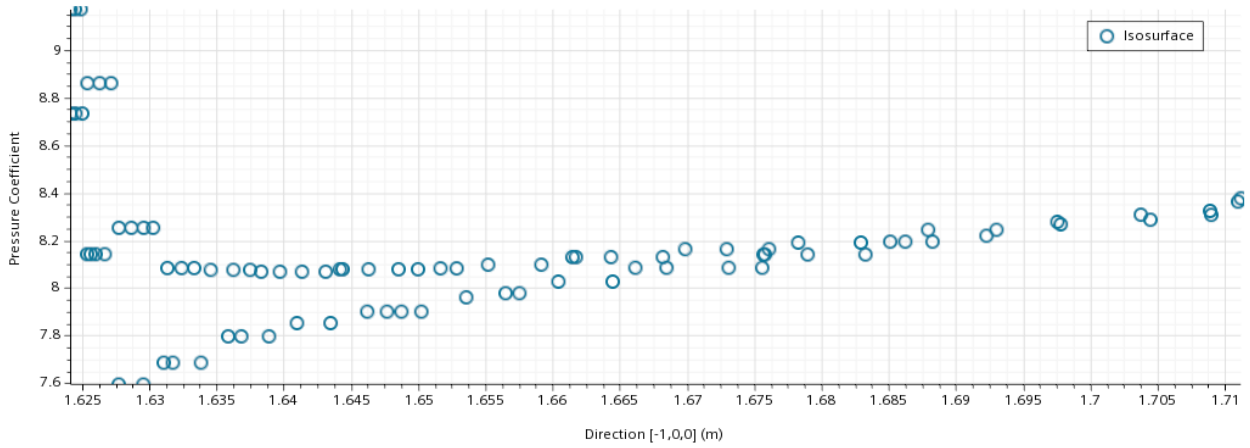

Figure 51: Beginners' design secondary wing's pressure coefficient distribution along the chord at 4^{o} of angle of attack

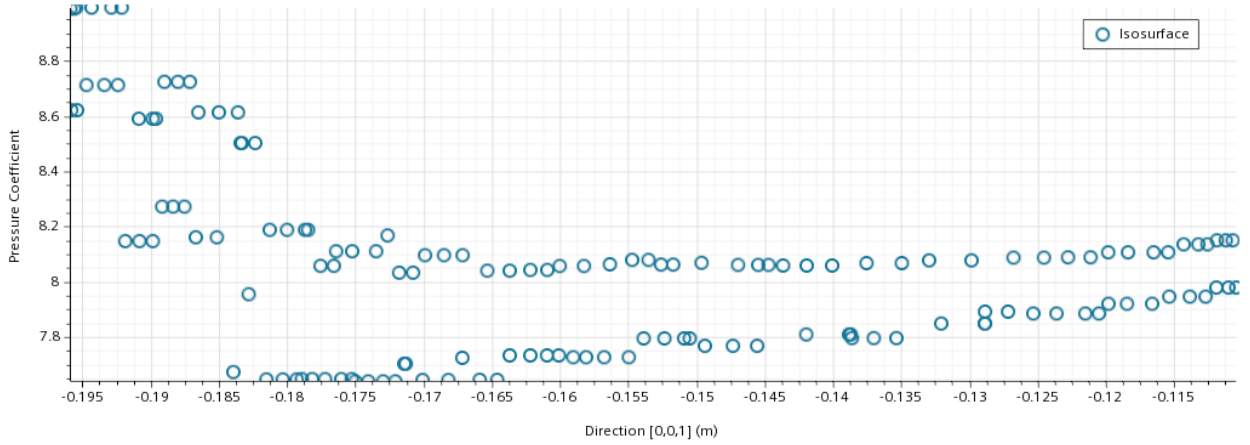

Figure 52: Beginners' design secondary wing's pressure coefficient distribution along the span at 4^{o} of angle of attack

When analyzing the wake the same conclusions mentioned before can be obtained by analyzing the results seen in Figure 53, the zone where the velocity is the lower, which will indicate a recirculation zone, is much bigger in size but also shows a different shape and even a zone at the center where there is no recirculation. This is because the secondary wing now is generating lift so the flow behaviour is more complicated since both wings generate downwash. This causes this pointed shape. Also, the no recirculation zone created in the middle is because of the different position between the fuselage's end and the secondary wing's trailing edge. Since, in his case, the fuselage will contribute to the lift, once the flow has travelled around the down side of the body, it follows the spherical shape flowing upwards and re-energizing the lower part of the secondary wing at the middle section thus avoiding the recirculation at this part.

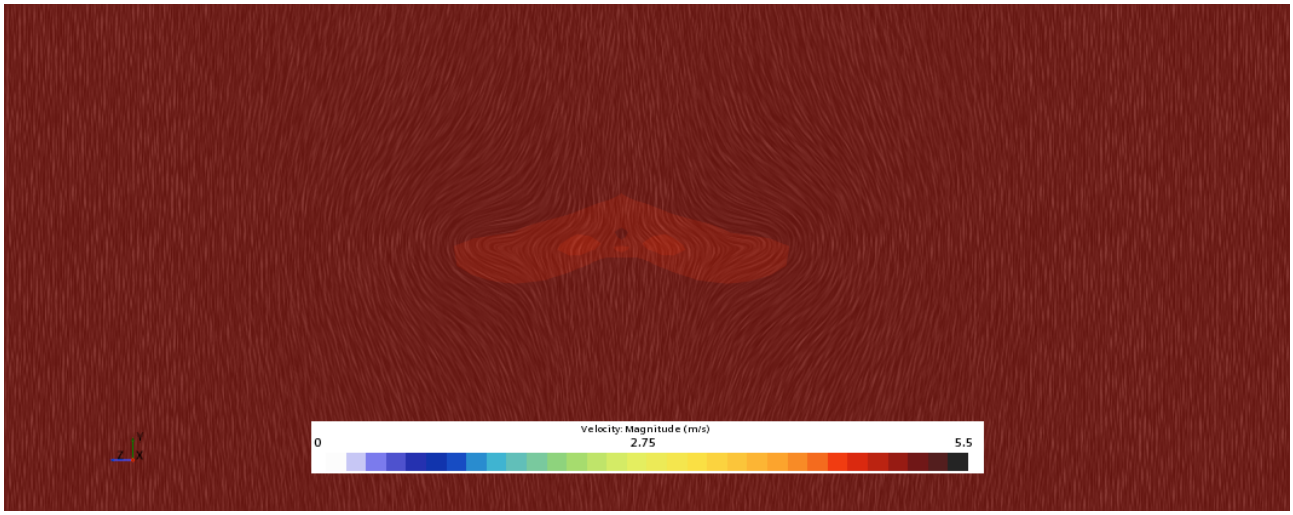

Figure 53: Beginners' design wake's front view velocity contour at 4º of angle of attack

Seeing the contours from the side point of view, in Figure 54, it can be seen how the stagnation point is now generated not in the symmetry line of the fuselage but in its lower part due to the increase in angle of attack. It can also be seen how the wake generated tends to go upwards due to the effect of the angle of attack as commented before. Also, from this point of view, it can be seen how the upper part of the fuselage shows a zone of higher velocity, cause of the lift generated by the fuselage. Other of the effects caused by the increase in angle of attack is how the boundary layer of the fuselage is not symmetric, showing a slightly higher thickness at the upper part since the displacement of the stagnation point forces the fluid to travel a longer distance losing more energy due to friction thus making the boundary layer to increasing its thickness.

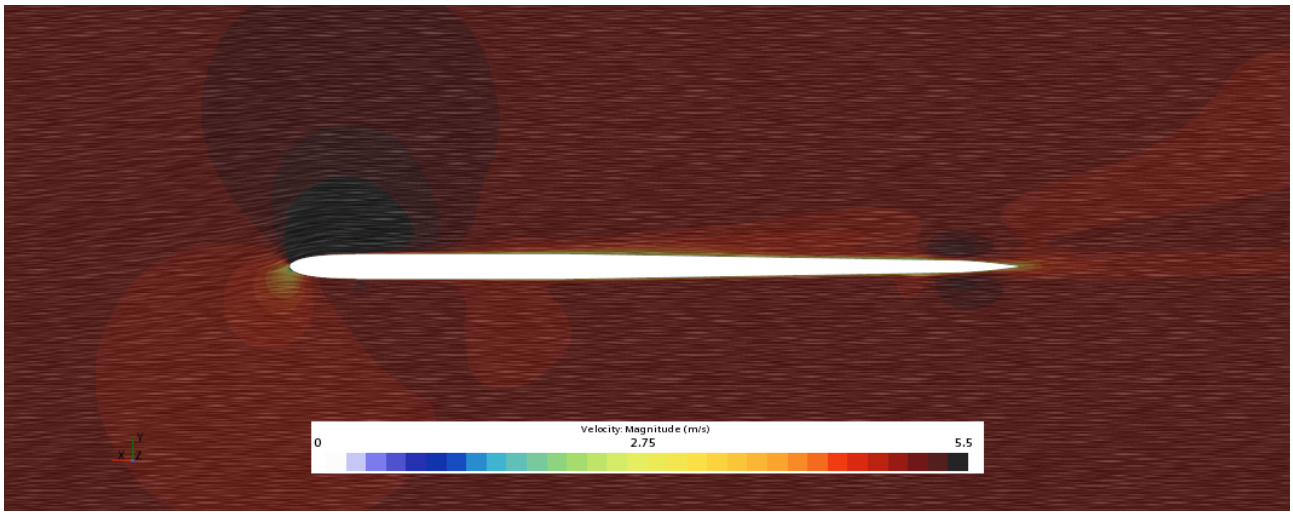

Figure 54: Beginners' design symmetry plane's side view velocity contour at 4º of angle of attack

When switching the plane towards the wingtip the same tendencies can be seen about the stagnation point location for both wings as seen in Figure 55. Also it can be seen how the

wake is generated with an angle upwards instead of at the horizontal. From this point of view it can also easily be seen how the secondary wing shows a higher velocity zone at its upper part, causing the negative pitching moment calculated before and contributing also to the lift increase seen.

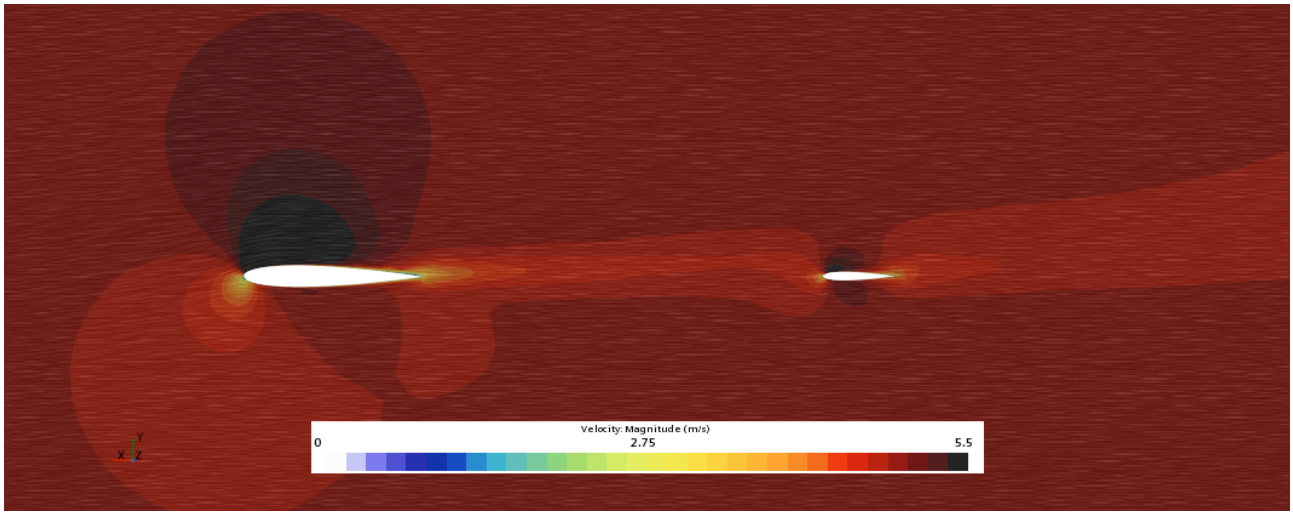

Figure 55: Beginners' design side view velocity contour at 4^{o} of angle of attack

After analyzing the geometry and how it affects the flow at different conditions it can be said that it accomplishes the list of requirements stated for this kind of design. It generates enough lift to lift up the pilot above water at a reasonably low speed, the secondary wing stabilizes the design at 0^{o} of angle of attack generating a small pitching moment in all the studied cases and has a significant lateral area due to the tips' design which stabilizes the geometry in roll and yaw movements.

6.2 Competition Design

This second design is aimed to professionals who are looking to compete in races or acrobatic challenges, so its objective is not to be easily controllable, since the pilot will be experienced enough, but to ease the pilot his or her performance in those scenarios. For obtaining this objective, different key points are needed:

- High pitching moment: the base movement of any kind of acrobatic is a jump, it is necessary that the pilot can easily take fly over the water. For being able to perform this maneuver, it is not necessary that the design is able to generate lift in the air and not in the water, but that the pitching moment generated is great enough for the pilot to be able to perform a jump by simply switching his or her weight to the foot behind and letting the design pitch up suddenly.

- High rolling and yawing maneuverability: the design has to be symmetric since it is necessary that it does not generate any rolling or yawing moment by itself, but the lateral area has to be minimum in order to give less opposition to the pilot control in yaw and roll.

- Low lift coefficient: since the design is aimed to perform at high velocities, it is necessary to achieve those velocities without lifting the whole geometry and its pilot above water or

generating cavitation zones around the geometry due to low pressure. This will mean that a higher velocity is needed in order to start a lift up of the pilot, but this can be controlled with the variables explained previously.

Once the list of requirements is done, it is possible to design an appropriate geometry.

6.2.1 Geometry's Description

Attending to the requirements list made previously, the final design can be seen in Figure 56 and is explained below.

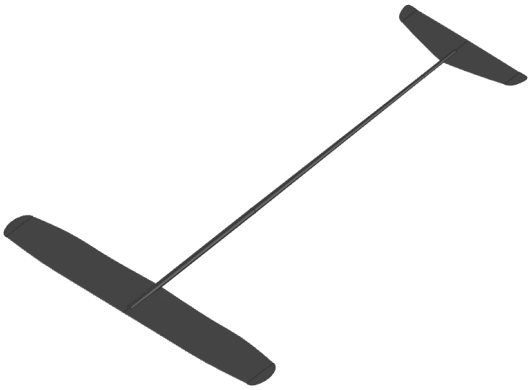

Figure 56: Competition design perspective view

Analyzing more in detail the design there are some features to be commented. Once again, the wingtips, which can be easily seen in Figure 57, are designed in order to reduce the induced drag by creating an elliptical wing, since in a race minimizing the drag generated is a key factor in order to improve the performance, an implicit requirement not mentioned in the list. Also, the symmetry of the design will ensure no rolling or yawing moment generation, satisfying in part the second requirement established (high yawing and rolling maneuverability).

Figure 57: Competition design top view

This requirement is completely fulfilled thanks to the thin lateral surface seen in Figure 58 and Figure 59. The thin lateral surface will ensure a low opposition to the inputs of the pilot when rolling or yawing.

Figure 58: Competition design front view

Figure 59: Competition design side view

The high pitching moment requirement is satisfied thanks to the secondary wing, which is designed with a symmetric profile with a variable geometric angle in order to generate a downwards force at a wider range of angle of attacks than a cambered profile, generating the desired pitching moment.

The design's characteristics are summarized in Table 8.

Main wing	
Profile	NACA0007
Maximum thickness	3.25 mm
Span	740 mm
Aspect ratio	14.19
Secondary wing	
Profile	NACA0003
Maximum thickness	1.75 mm
Span	350 mm
Aspect ratio	11.47
Fuselage	
Length	1050 mm

Table 8: Competition geometry main characteristics

Both wings are designed with a symmetrical profile with a geometrical angle respect to the horizontal plane. In the case of the secondary wing, the profile starts being symmetric and is torsioned reaching an angle of -3º at 50 mm from the symmetry plane in order to generate the downwards force needed to create pitch, that torsion is maintained for the rest of the span. For the main wing, the torsion is generated in order to reach an angle of 2.5º at 100 mm from the symmetry plane, maintaining this angle for 100 mm and going back to 0º when reaching the tips. This torsions can be seen in Figure 58. The distances between the symmetry plane and the maximum torsion angle have been selected in order to minimize the fuselage interferences, since a more cambered profile will be less adaptable to the impact the fuselage has on the flow. For the fuselage, it consists of a cylinder with two rounded extremes in a spherical way which extends in length between the points of maximum thickness of both wings, being its diameter 6.5 mm at the main wing's side and 4 mm at the other extreme. The high fuselage's length is done in order to create more pitching moment by means of the secondary wing.

The design obtained in order to meet the requirements may mean some structural challenges due to the reduced size of the bodies created but they can be easily solved. The structural analysis is out of the scope of this project but, considering the performance level of the design, high quality materials could be used without any cost problem, since the customer aimed is expected to be willing to spend as needed in order to obtain a high performance product.

6.2.2 Geometry's Analysis

Note that, although the analysis procedure will be the same between the both designs, there is no intention of comparing them both, each one has a concrete function and is designed following different criteria.

The first task is to study the quality of the mesh generated around the geometry. Due to the low thickness of the geometry, a close-up of the most critical parts, the wings, is shown in Figure 60 and Figure 61. As it can be seen, there is no zone where the global cells or the prism layer cells show a non-regular shape, they follow the parameters established previously in this document.

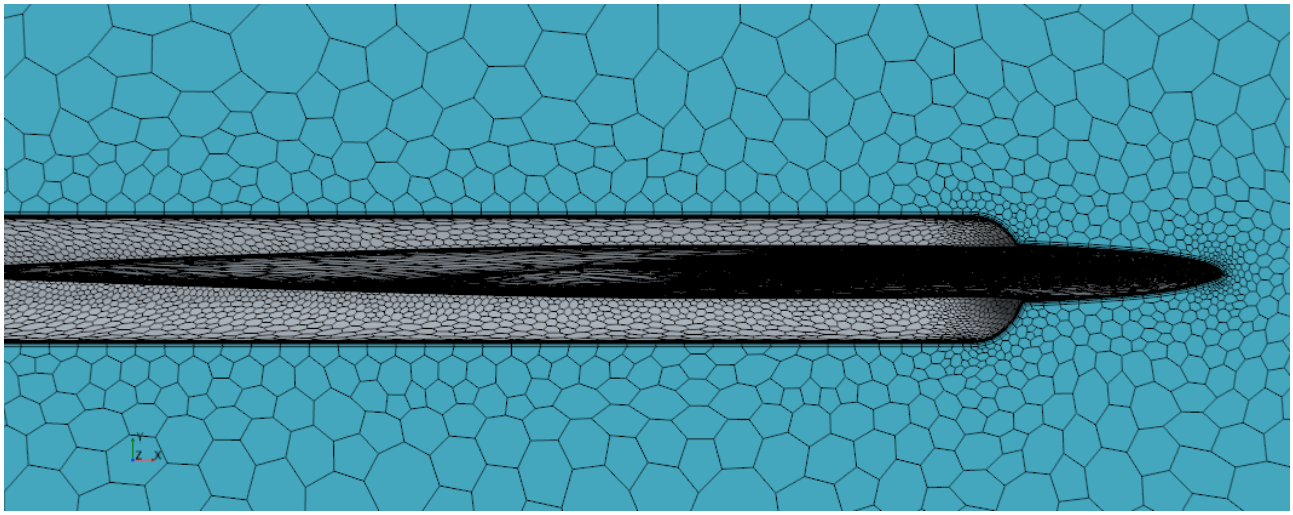

Figure 60: Competition design main wing mesh side view close up

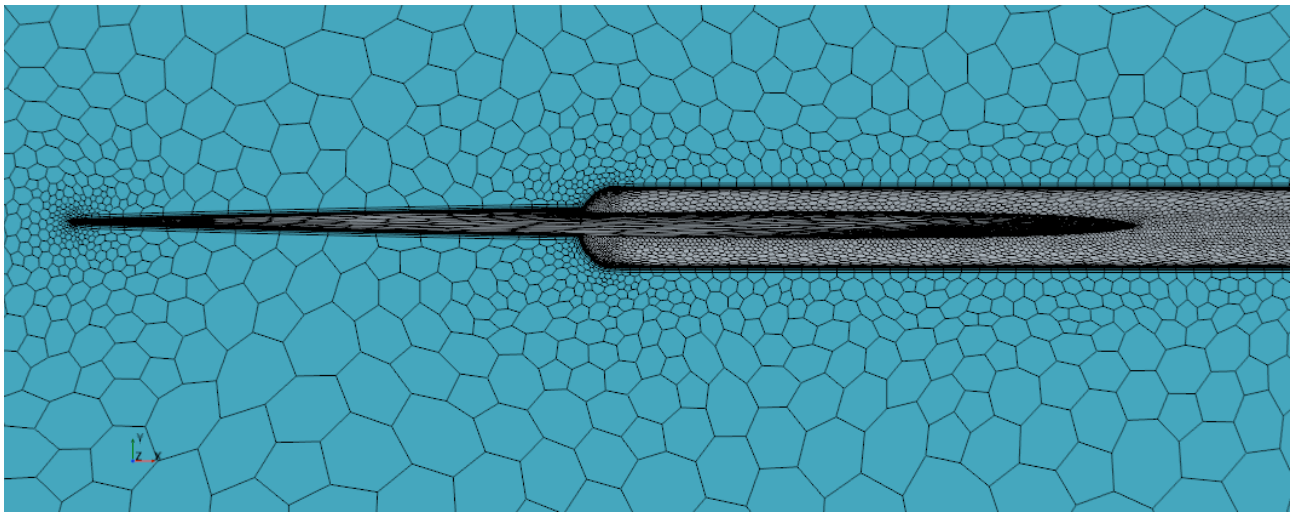

Figure 61: Competition design secondary wing mesh side view close up

Switching to a front point of view in order to check the mesh generated around the tips, Figure 62 and Figure 62 show how the global cells and the prism layer cells adapt properly to the geometry fulfilling the requirements stated previously. Note that, due to the reduced size of the geometry, in Figure 63 the view has been zoomed in for properly seen the cells created.

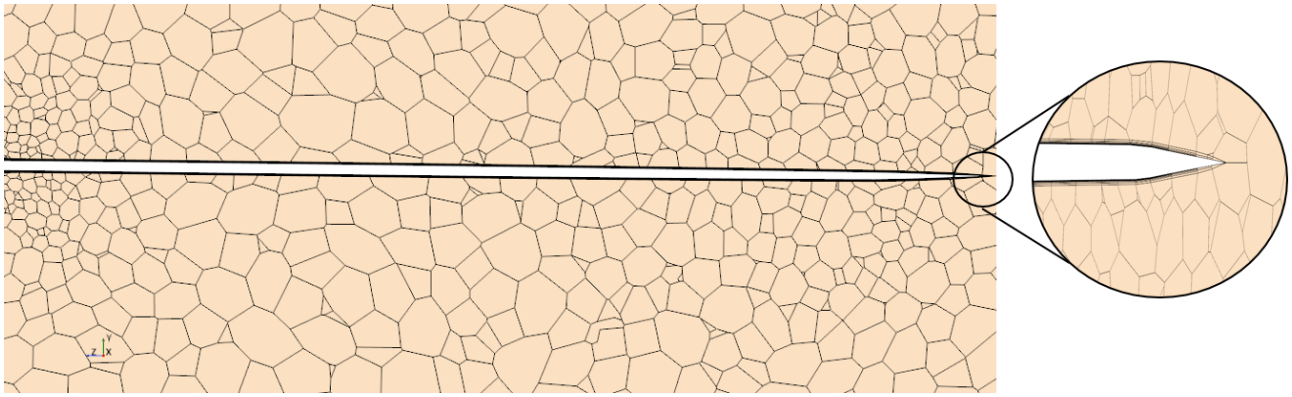

Figure 62: Competition design main wing mesh front view

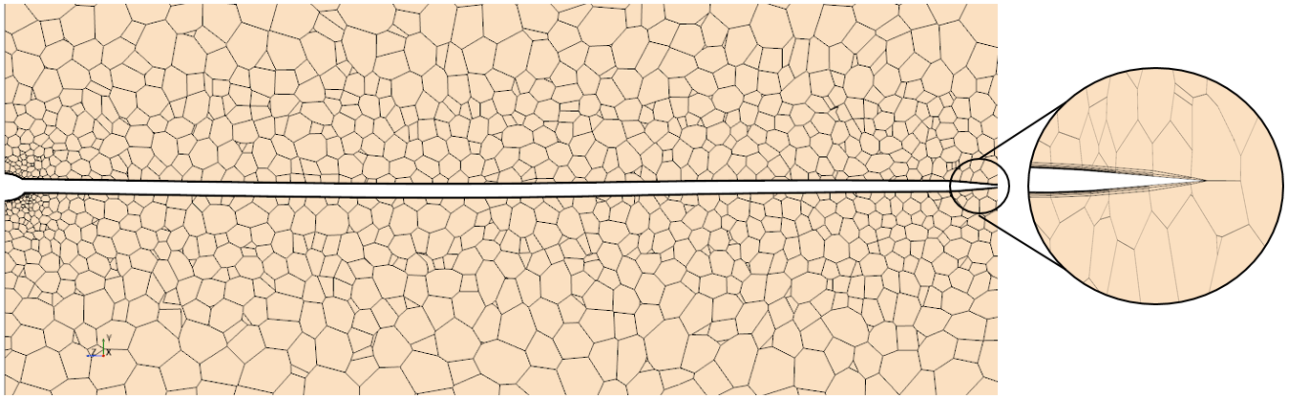

Figure 63: Competition design secondary wing mesh front view

Once the mesh quality has been confirmed, the analysis of the flow behaviour around the geometry can be done. Starting with the forces and pitching moment study at different velocities, once again expressing the velocities in knots and the lift in its equivalent mass.

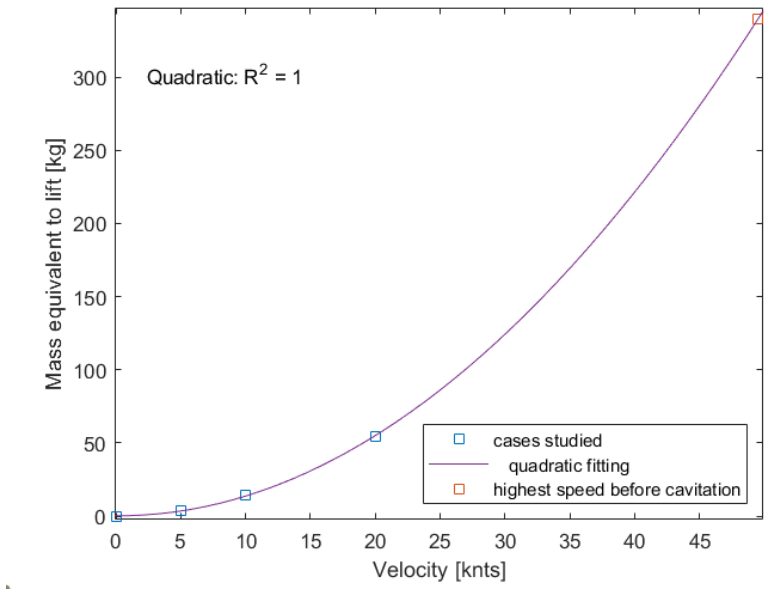

Figure 64: Mass equivalent to lift generated at different velocities for competition design

In Figure 64 it can be seen how the lift increases slowly with velocity, needing high velocities to lift considerable masses. This fulfills the low lift coefficient requirement and allows the pilot to reach higher velocities without being completely lifted up thus losing the lift generated since the hydrofoil would be above water.

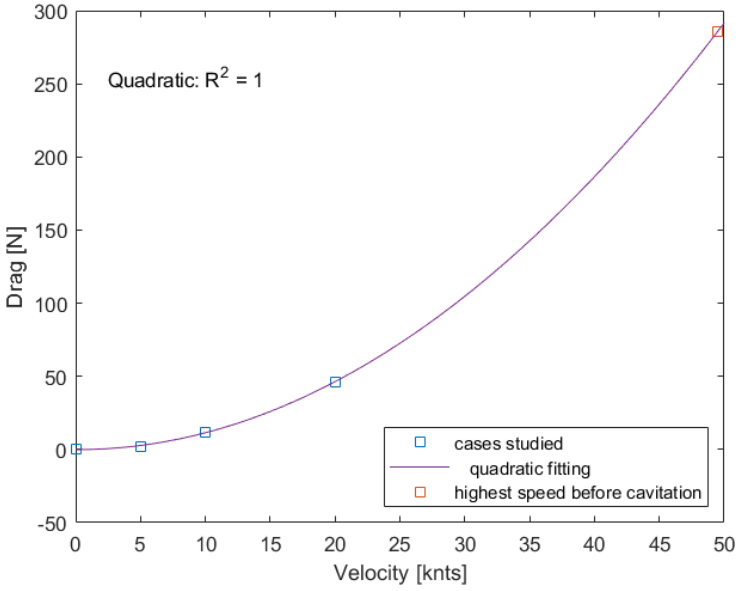

Figure 65: Drag generated at different velocities for competition design

Once again, in Figure 65 it can be seen how the lift increases in a slower way than the lift. With the data obtained from Figure 64 and Figure 65 the efficiency can be calculated for a velocity value high enough to lift the 70 kilos stated obtaining a value of 11.7. This high value

of efficiency would be an implicit requirement for a competition design since the velocity is a key factor.

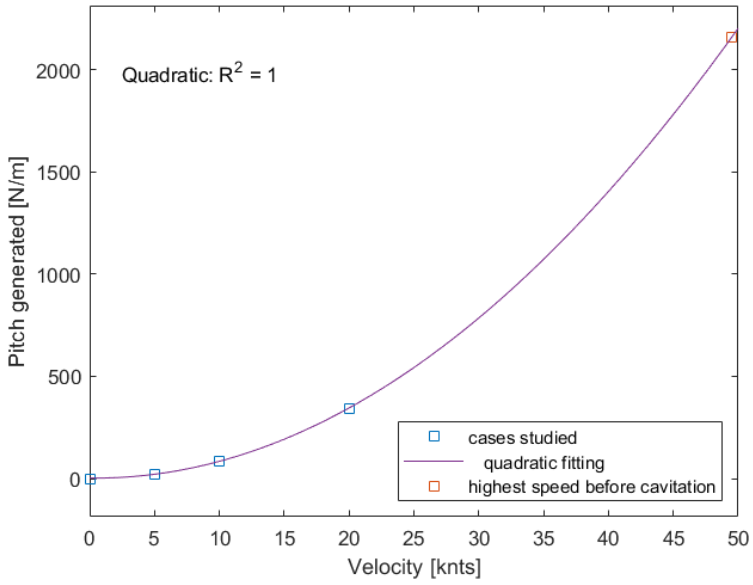

Figure 66: Pitching moment generated at different velocities for competition design

When analyzing the pitching moment in order to check the fulfillment of the high pitching moment requirement, in Figure 66 it can be seen how the pitching moment increases drastically with speed, reaching high values. The requirement can be considered as fulfilled, the pitching moment generated will ease performing acrobatics.

Once again, the three graphs seen in Figure 64, Figure 65 and Figure 66 follow the expected quadratic shapes. Also, from these graphs it can be calculated that the cavitation speed is 49.5 knots (or 25.47 meters per second), which is a velocity high enough for considering the cavitation not a problem even in races where the velocity is a key factor. Also, the velocity needed to generated the 70 kilos previously stated is of 22.55 knots (or 11.6 meters per second). At this velocity further studies about the flow behaviour will be performed.

Competition design analysis: 22.55 knots no angle of attack no roll

Starting, as stated, with the analysis at 0° of angle of attack and the 22.5 knots of speed, analyzing first the vorticity, in Figure 67 and Figure 68, it can be seen how the elliptical wingtips reduce the vorticity generated at both sides of both the main and secondary wing, being the zone with a bigger wake the one behind the fuselage due, once again, to its length and spherical-shaped ending.

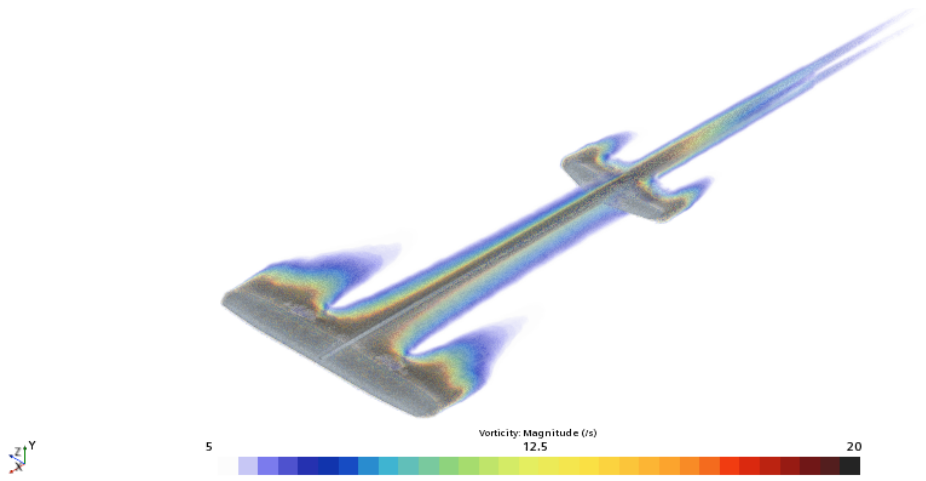

Figure 67: Competition design vorticity contour

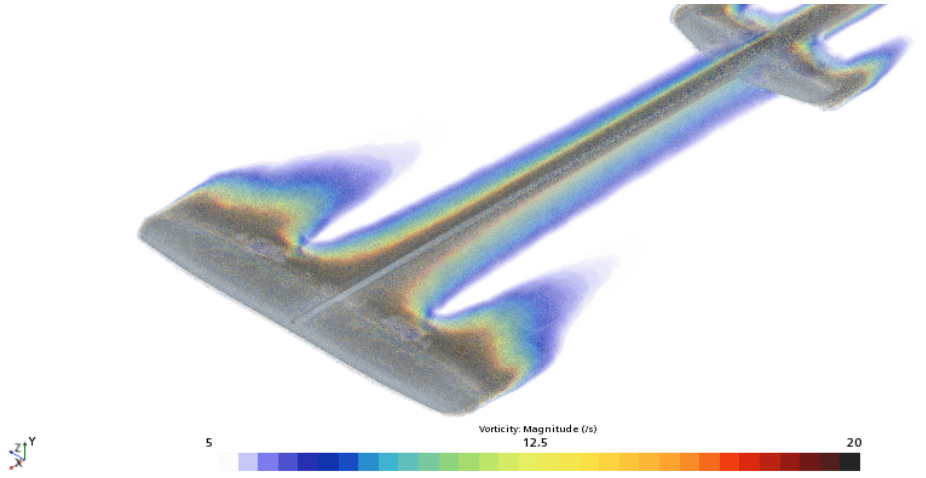

Figure 68: Competition design close up vorticity contour

Studying now the velocity contours, starting with the front view of the main wing, in Figure 69 it can be seen how the higher velocity zone is generated at the upper part of the wing, creating a suction zone which, together with the higher pressure zone generated at the lower part of the wing, will generate the lift. It can also be seen how the wingtip vortex is still generated although the wingtips elliptical shape will reduce its intensity as seen before.

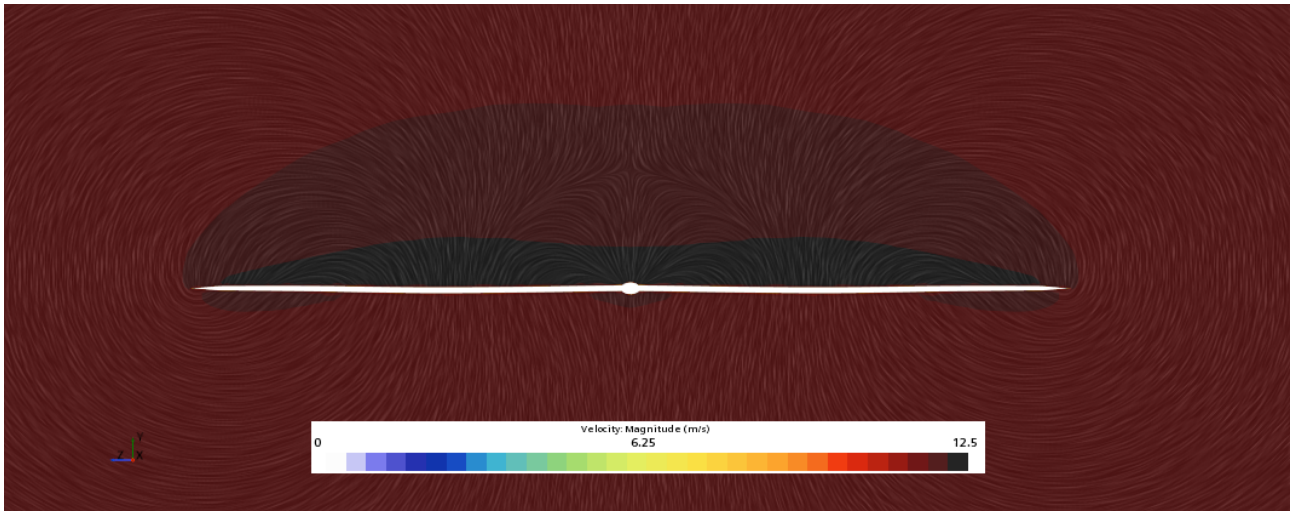

Figure 69: Competition design velocity contour main wing's front view

Switching the focus to the secondary wing, in Figure 70 it can be seen how, in this case, the suction zone is generated at the lower part of the secondary wing. This is because of the design of the secondary wing which has been done attempting to create a downwards force, responsible of generating the pitching moment seen in Figure 66 and stated as a requirement. Also, in this case, the wingtip vortex of the secondary wing can not be seen because is attenuated by the main wing's wingtip vortexes, which is generated in an opposite rotating direction.

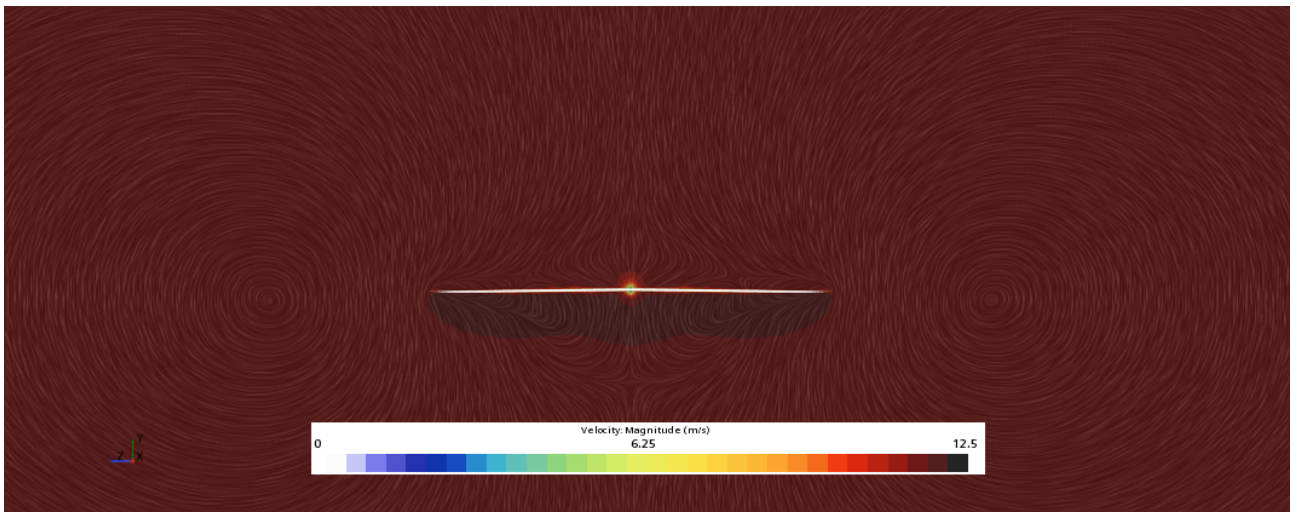

Figure 70: Competition design velocity contour secondary wing's front view

When studying the wake generated, from Figure 71 it can also be concluded that the fuselage, due to its length and shape, is the responsible of the lower velocity zone seen in the center of the image, while the secondary wing generates the lower velocity zone which extends along the span. It can also be seen the interaction between the both wingtip vortexes affecting the flow trajectory.

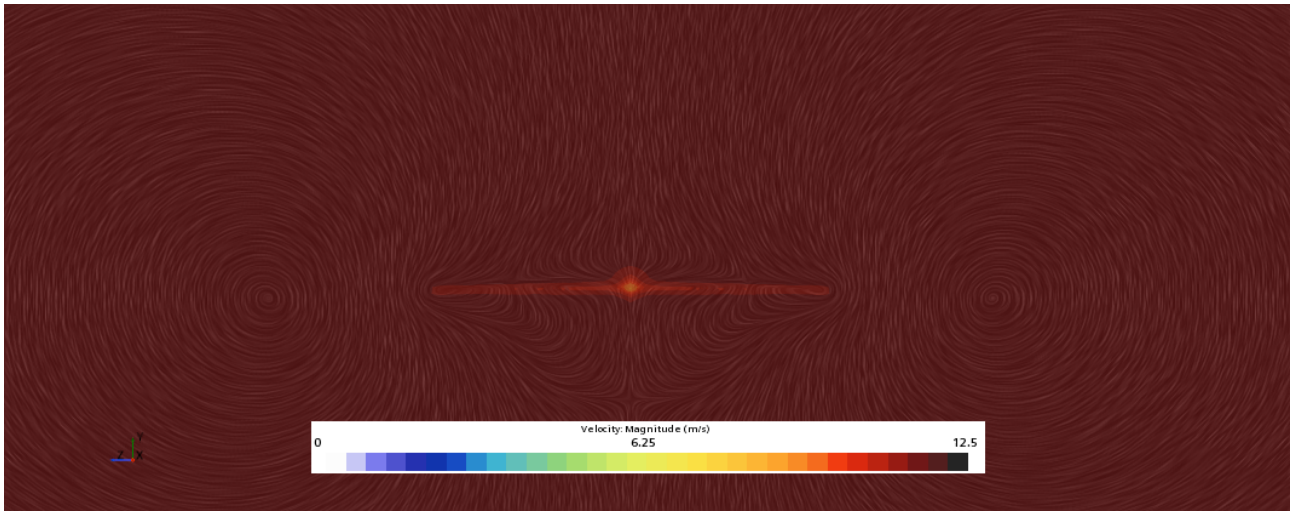

Figure 71: Competition design velocity contour wake front view

This same behaviour can be seen from the side in Figure 72, where the recirculation zone can be seen behind the fuselage, as seen, more in detail, in Figure 73. Another remarkable event takes place at the leading edge of the fuselage. It can be seen how a high velocity zone is created due to the interference of the main wing and the fuselage front spherical end. Since the flow is first disrupted by the main wing's leading edge, which is thinner than the fuselage, the stagnation point is created at the main wing and not the fuselage and, when the flow arrives to the higher section, which is the fuselage, the change perceived by the fluid is not so abrupt to detach the boundary layer or to create a new stagnation point, but is perceived as an increase in the wing's size and the velocity is increased due to this change in size. Obviously, the spherical end of the fuselage contributes to this phenomena, a less smooth end would make the change in the conditions perceived by the fluid more abrupt and would increase the possibilities of a boundary layer detachment.

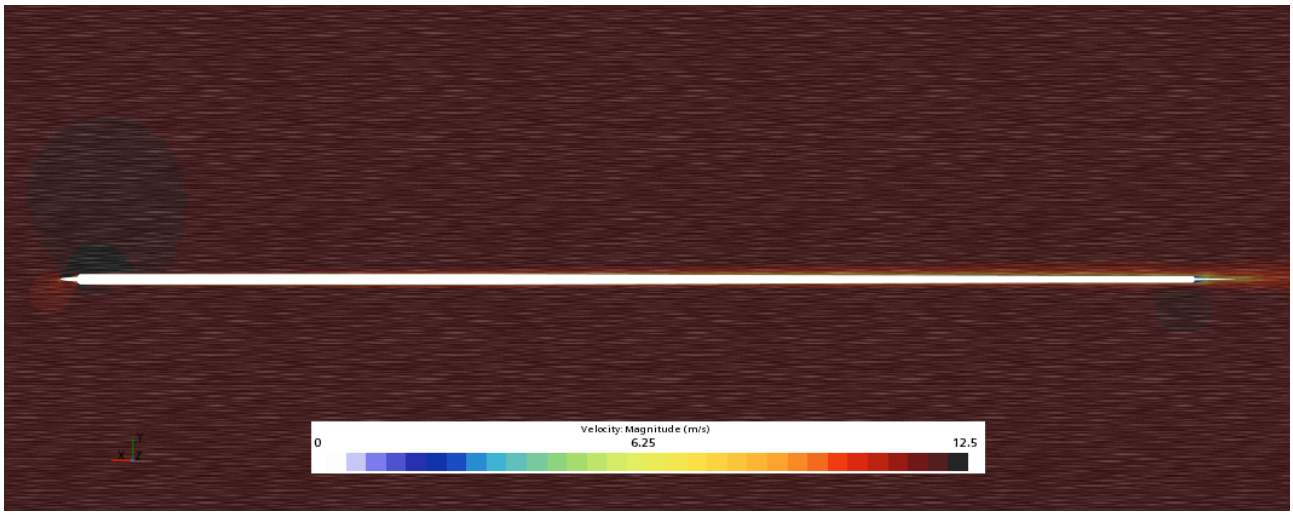

Figure 72: Competition design velocity contour symmetry plane view

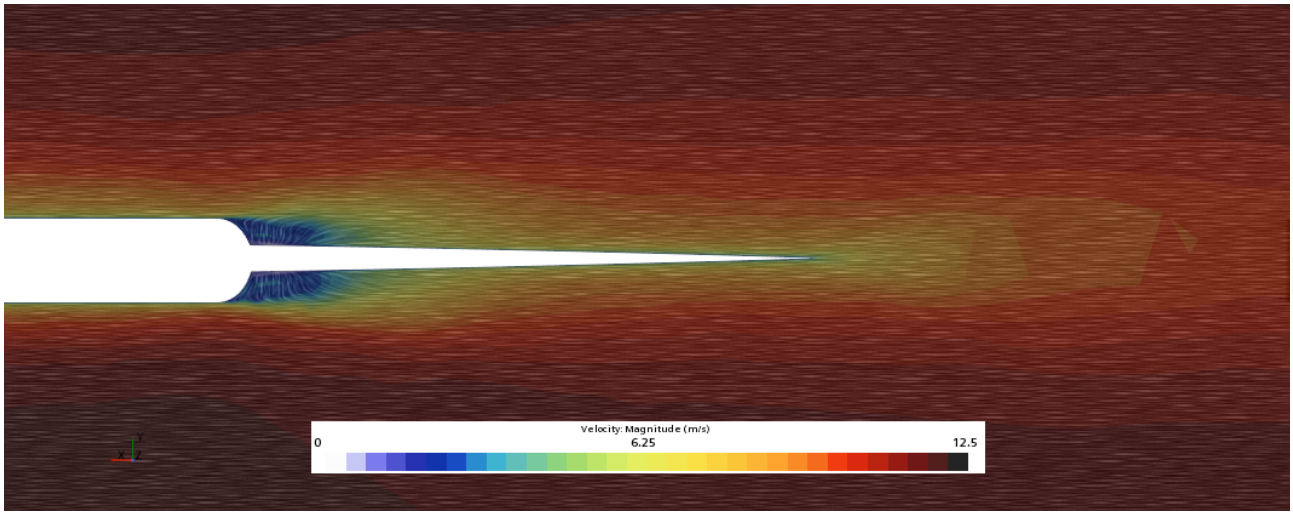

Figure 73: Competition design close up velocity contour symmetry plane view

When moving the studied plane towards the tip, in Figure 74 it can be seen how the low velocity zone created at the lower part of the main wing is extended as the main wing's downwash. For the secondary wing, this low velocity zone is placed at the upper part of the secondary wing, which is generating a negative lift or a downwards force. This zone is bigger for the main wing due to the geometry's bigger surface.

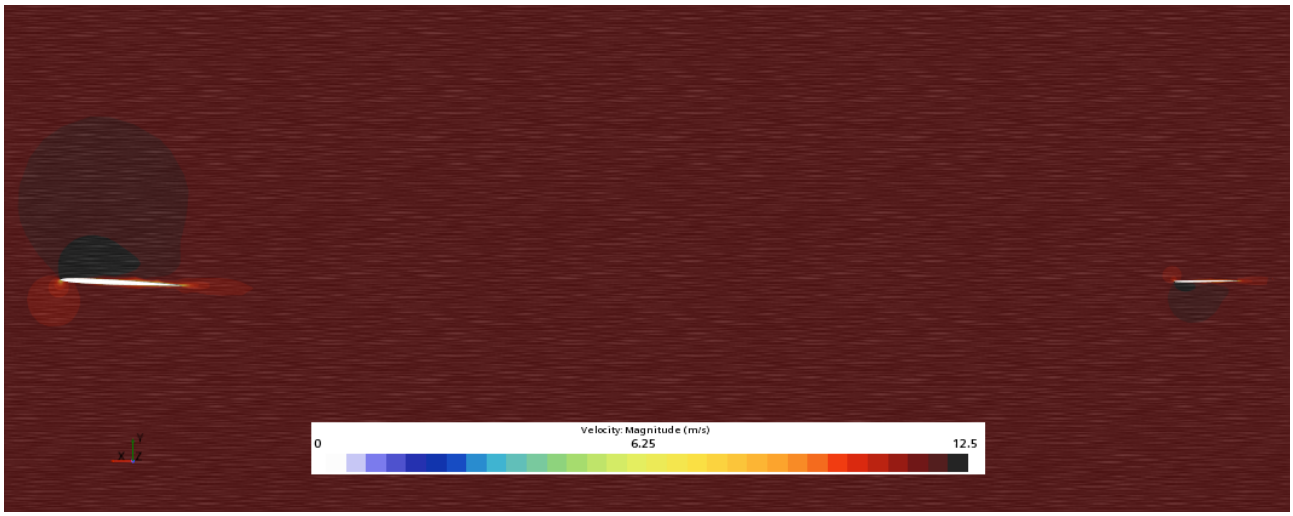

Figure 74: Competition design velocity contour side view

Competition design analysis of roll angle

The next step in the analysis is, without varying either the velocity or the angle of attack, to add a roll angle of 15^{o} in order to simulate a right turn performed by the pilot. Note that, once again, the symmetry is lost and all the study has to be performed for the whole geometry, not only one side. The results obtained for the main forces and pitching moment are seen in Table 9.

Lateral force	Upwards force	Drag	Pitching moment
175.18 [N]	655.18 [N]	64.35 [N]	425.19 [N/m]

Table 9: Competition geometry at 15º of roll main forces and moment

As done before, the first analysis will be the vorticity scene seen in Figure 75. The wake generated is not symmetrical since the right wing (which is lower) generates a wider wake because of the lateral component of the flow. Note that this effect is enhanced due to the small lateral area, which eases the extension of the wingtip vortexes on the upper part of the wing. In this case, the wake generated is placed behind the whole secondary wing instead of focused behind the fuselage.

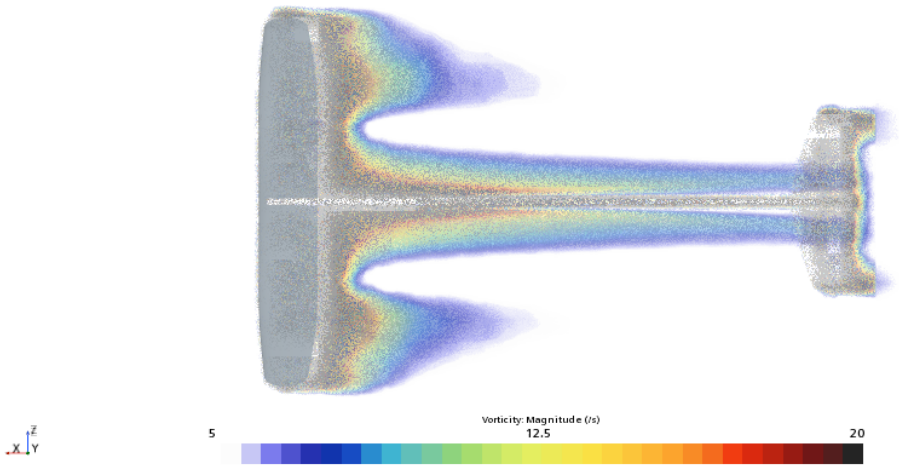

Figure 75: Competition design vorticity contour at 15º of roll

Following the same procedure already used, analyzing the velocity contour from a front point of view, in Figure 76 it can be seen how the suction zone extends above the main wing, generating a force normal to the surface which can be decomposed into a lateral and a vertical one as seen in Table 9. It can also be seen how the flow follows different trajectories in each wingtip but with a similar behaviour since both are wingtip vortexes.

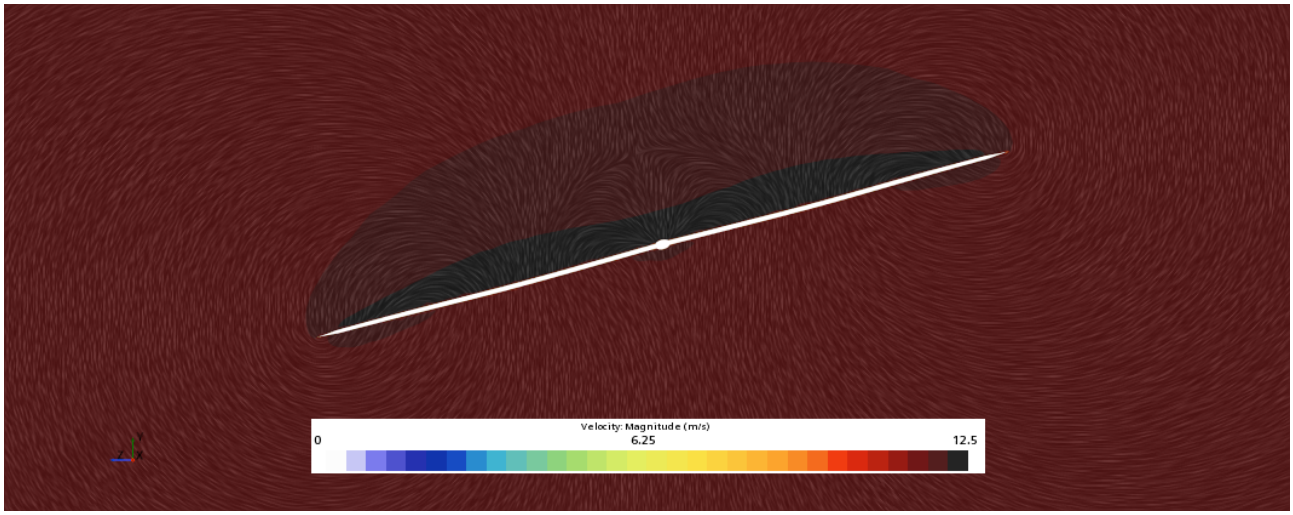

Figure 76: Competition design's main wing front view velocity contour at 15º of roll

Moving to the secondary wing in Figure 77, it can be see how in this case the suction zone is still placed below the wing in order to generate the pitching moment required and seen in Table 9. It can also be seen how the main wing's wingtip vortexes extend until the secondary wing.

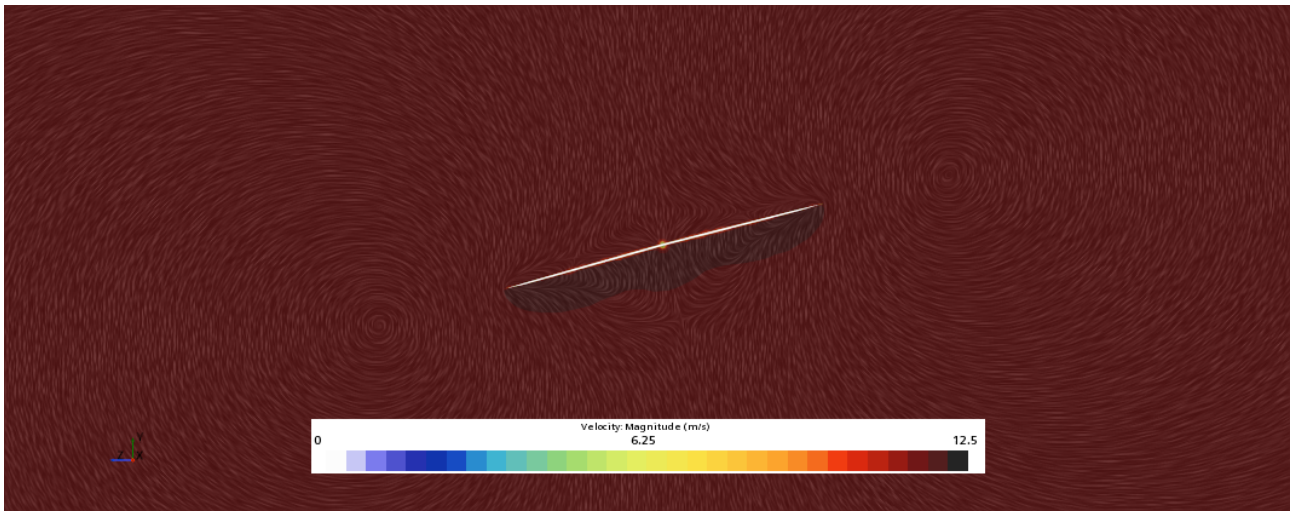

Figure 77: Competition design's secondary wing front view velocity contour at 15º of roll

When analyzing the wake generated, in Figure 78 it can be seen how a lower velocity zone extends for the whole secondary wing's span, being reduced as it gets closer to the wingtips as stated before when analyzing Figure 75. It also can be seen how the high velocity zone placed under the secondary wing still extends immediately after the fluid has travelled around the whole secondary wing.

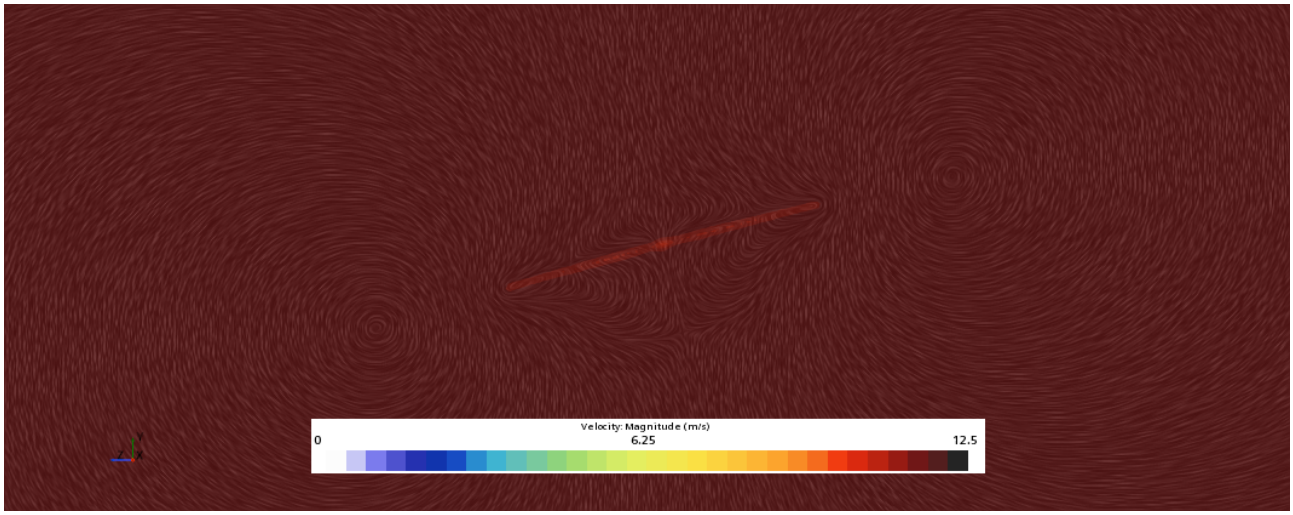

Figure 78: Competition design' wake front view velocity contour at 15º of roll

Analyzing the side view of the geometry, in both Figure 79 and Figure 80 it can be still seen the asymmetry on the flow behaviour. The right side of the geometry presents a bigger zone of low velocity under the main wing and a slightly smaller wake. When talking about a higher velocity zones (suction) both sides present a similar behaviour. Also, it can be once again seen how the higher velocity zone placed below the secondary wing still extends downstream after the secondary wing has been completely travelled by the fluid.

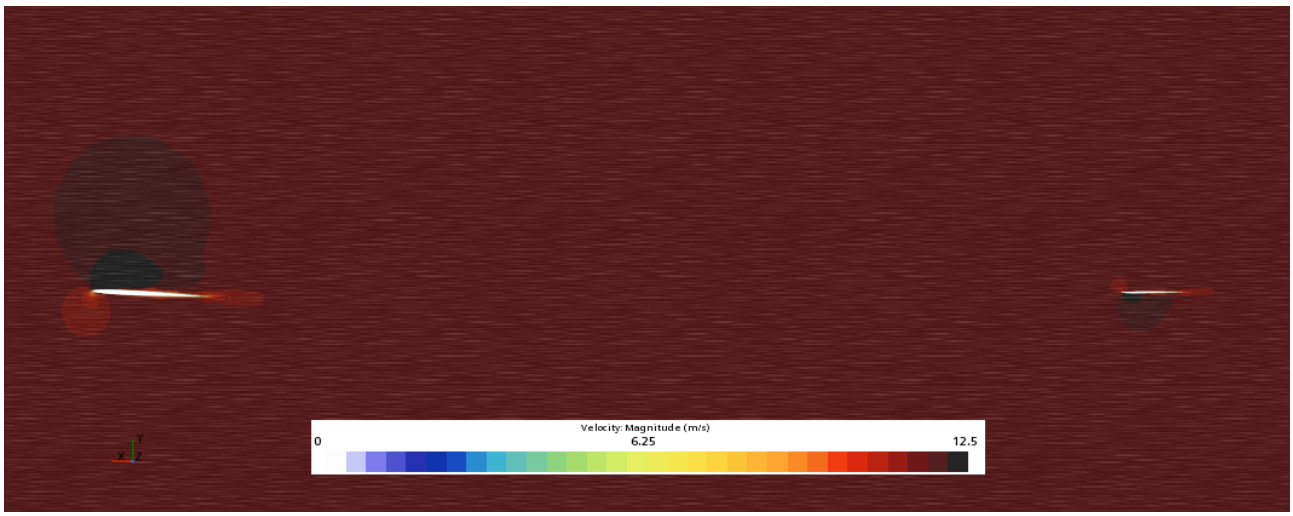

Figure 79: Competition design right side view velocity contour at 15º of roll

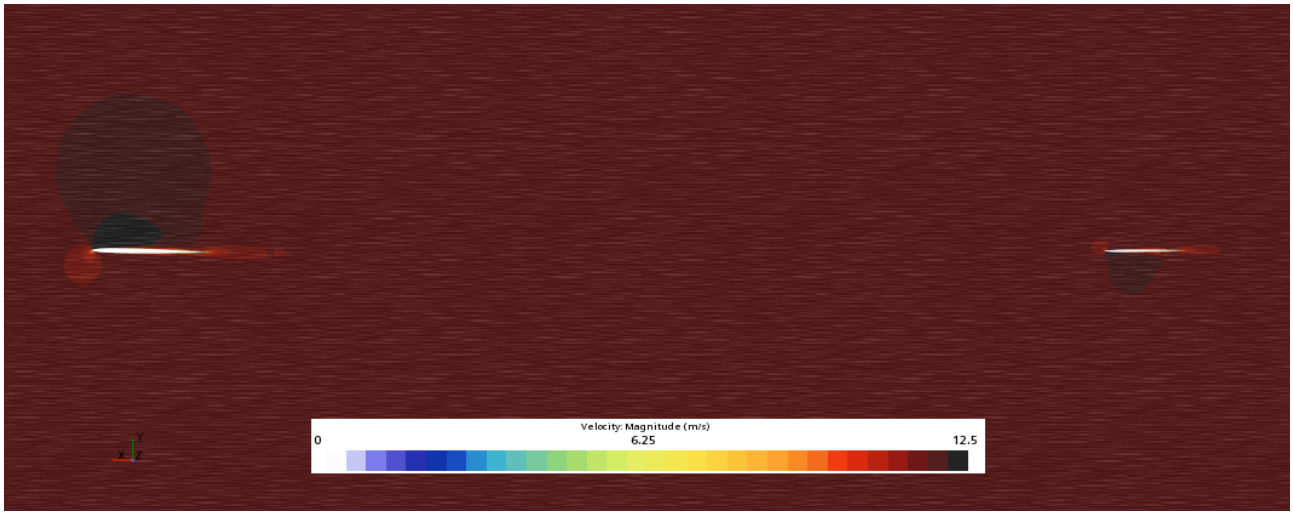

Figure 80: Competition design left side view velocity contour at 15º of roll

In the middle part of the geometry, in Figure 81 the suction zones due to both of the wings can be seen placed at the main wing's upper part and secondary wing's lower part as seen before. Also, in Figure 82 it can be seen how the recirculation zone behind the fuselage is reduced respect to the no roll scenario due to the lateral component of the flow..

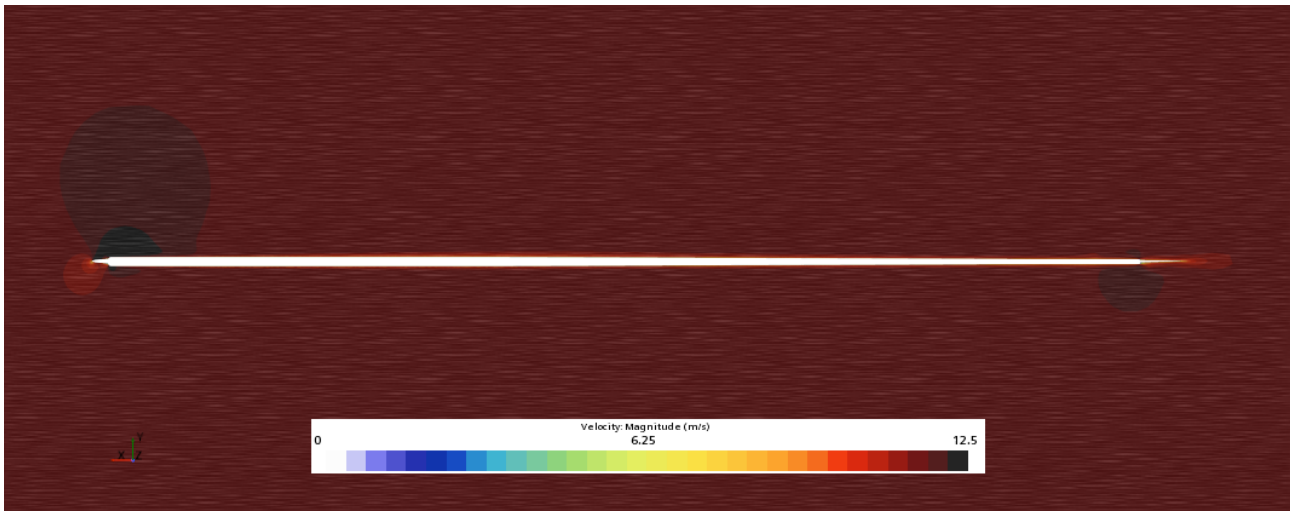

Figure 81: Competition design symmetry plane side view velocity contour at 15º of roll

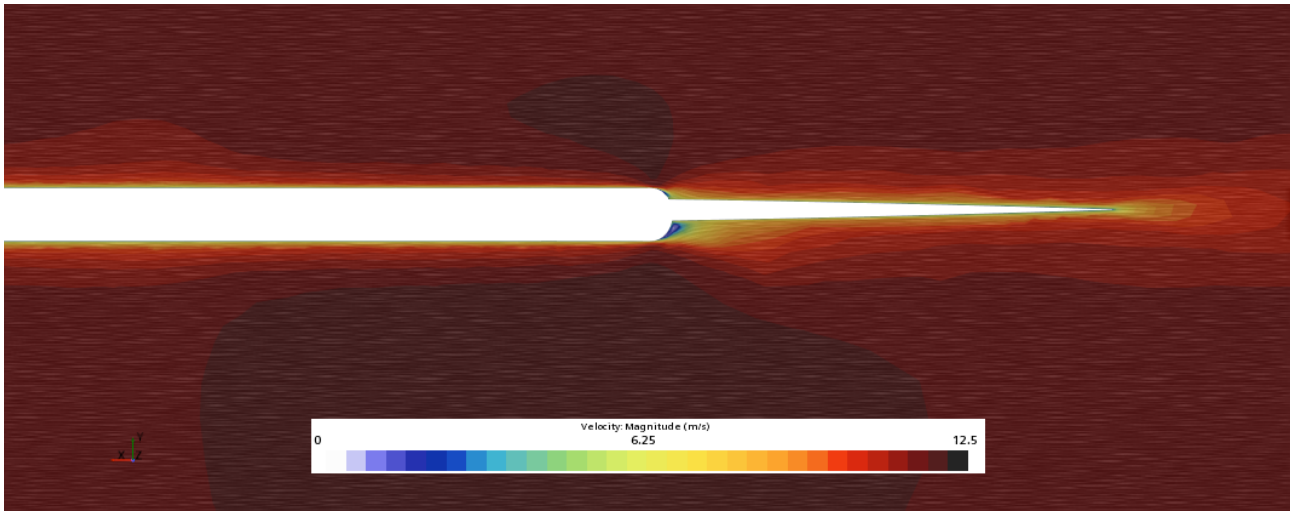

Figure 82: Competition design close up symmetry plane side view velocity contour at 15º of roll

Competition design analysis of angle of attack effect

The next scenarios studied will be, as stated before, the combination of increasing the angle of attack and decreasing the flow velocity in order to reach a lift equivalent to approximately 70 kilos, aiming to reach the minimum velocity possible without provoking a boundary layer detachment due to a extremely high angle of attack or low velocity. The conditions and results of this study are seen in Table 10.

Angle of attack	Velocity	Lift	Drag	Pitching moment	Efficiency
2.5 [º]	14 [knts] = 7.2 [m/s]	756.28 [N]	42.76 [N]	323.74 [N/m]	17.69 [-]

Table 10: Competition geometry angle of attack main forces and moment

When increasing the angle of attack to just 2.5º the velocity needed to lift the approximately 70 kilos stated is reduced from 22.5 knots to just 14 knots. This is because of several reasons, first of all, now the whole main wing is generating lift (the symmetry section around the fuselage does not contribute to the lift generation at 0º of angle of attack, but when it is increased it starts to generate lift), secondly, the torsioned part of the main wing now perceives obviously a higher angle of attack thus generates a higher pressure difference and a higher lift, and, lastly, the secondary wing was torsioned in a negative angle, so increasing the angle of attack reduces the magnitude of the negative force generated by the secondary wing. This last reason affects to both the lift (increasing it) and the pitching moment (reducing it).

As done before, starting with the analysis of the vorticity, in this case the elliptical wing still reduces the formation of big wake zones at the wingtips, also, the main wake zone is behind the fuselage but the vorticity increases in its magnitude in the main wing due to the higher lift generation.

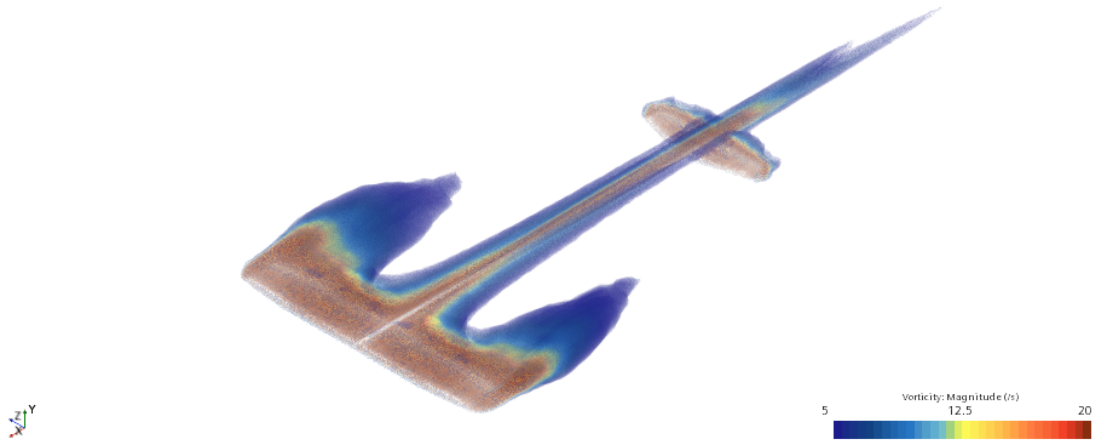

Figure 83: Competition design vorticity contour at 2.5º of angle of attack

In Figure 84 it can be seen how a great zone of higher velocity (a suction zone) is formed at the upper pat of the wing and a lower velocity zone is generated at the lower part of the wing. These both zones are the cause of the lift generated. Once again, the wingtips elliptical shape causes the wingtip vortexes to be reduced.

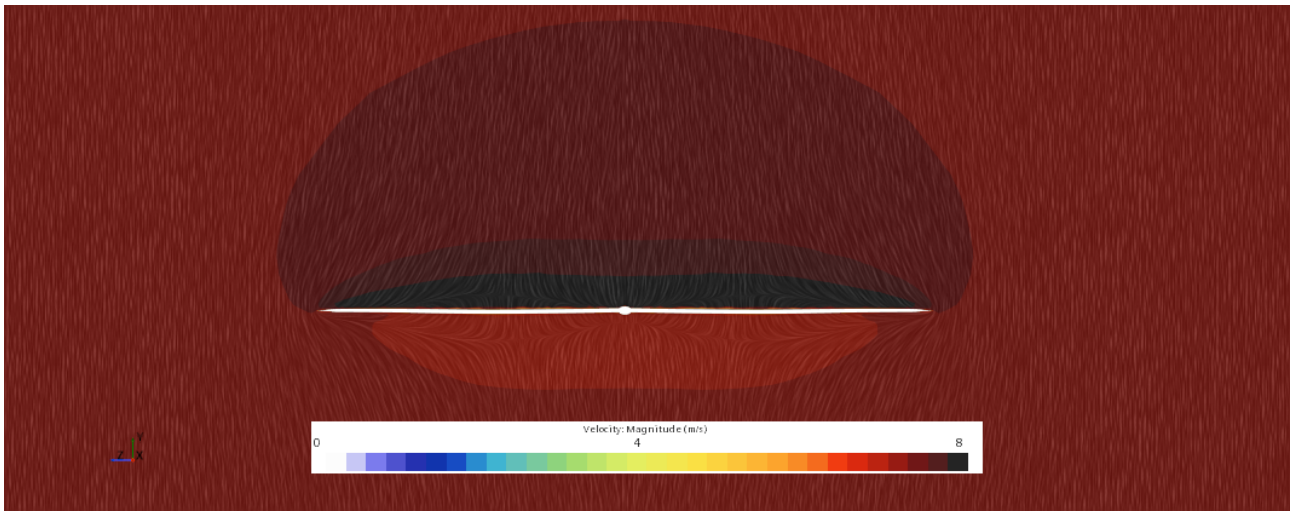

Figure 84: Competition design main wing's front view velocity contour at 2.5º of angle of attack

In the secondary wing, seen in Figure 85, zones of higher velocity can be seen, both at the top and the bottom of the wing. This is due to the torsion in the geometry, which was of a -3º, so now, with the 2.5º increase in angle of attack, the resultant is a symmetrical profile which perceives an angle of attack of about -0.5º, so the secondary wing will not generate a big pressure difference. The fact that the resultant angle is negative, added to the effect of the downwash produced by the main wing (which also affects the angle of attack) is the cause of the pitching moment, since the secondary wing generates a much smaller force than the main wing. For properly see the different velocities zones formed around the secondary wing a different contour will be studied.

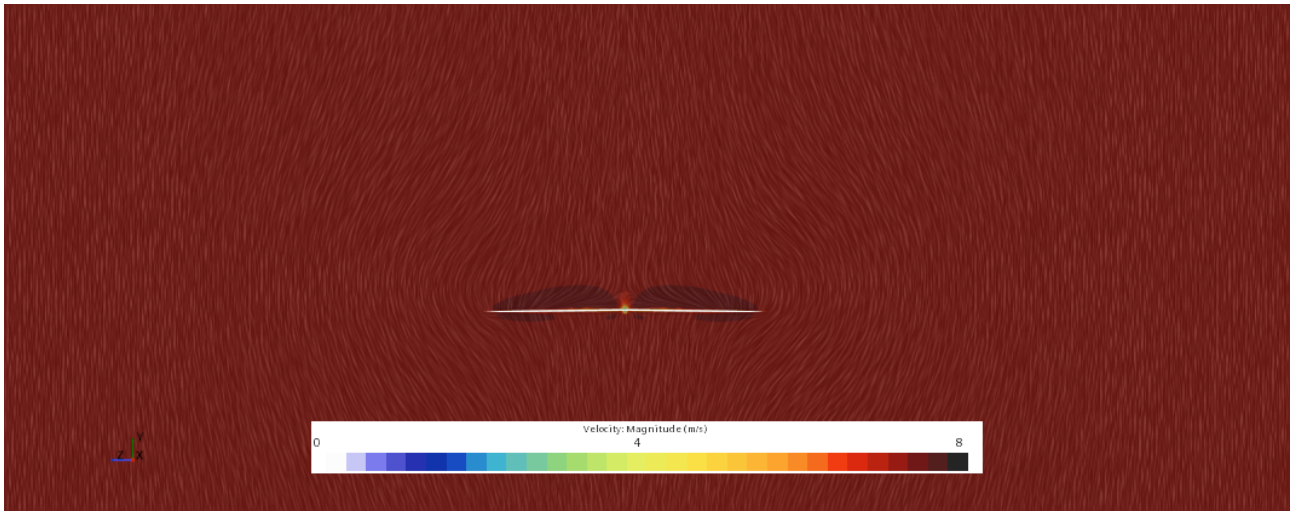

Figure 85: Competition design secondary wing's front view velocity contour at 2.5º of angle of attack

In Figure 51 and Figure 87 it can be seen in a more detailed way the pressure difference generated between the top and bottom parts of the secondary wing. As it can be seen, there is a small pressure difference, which is the cause of the pitching moment calculated in Table 10.

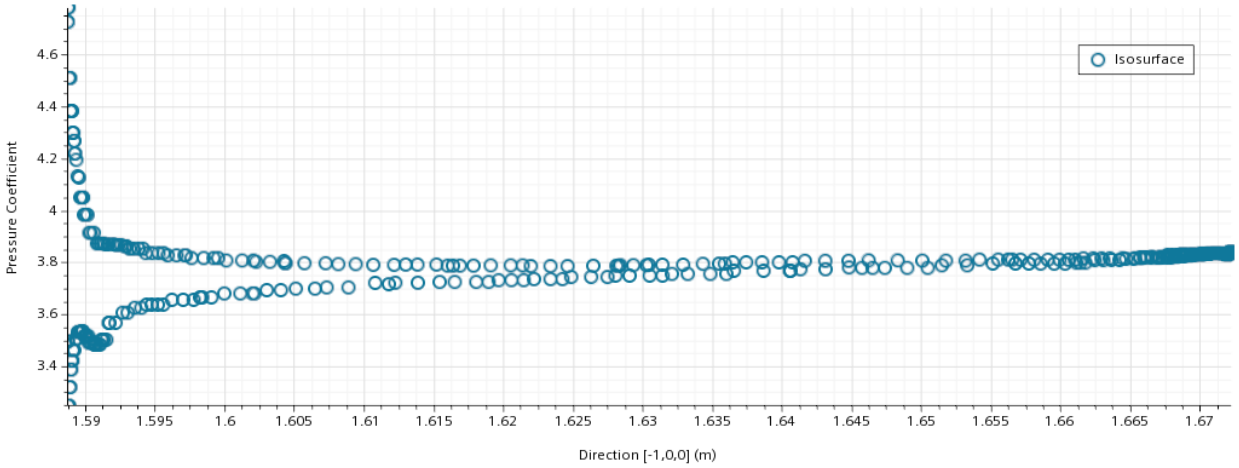

Figure 86: Competition design secondary wing's pressure coefficient distribution along the chord at 2.5º of angle of attack

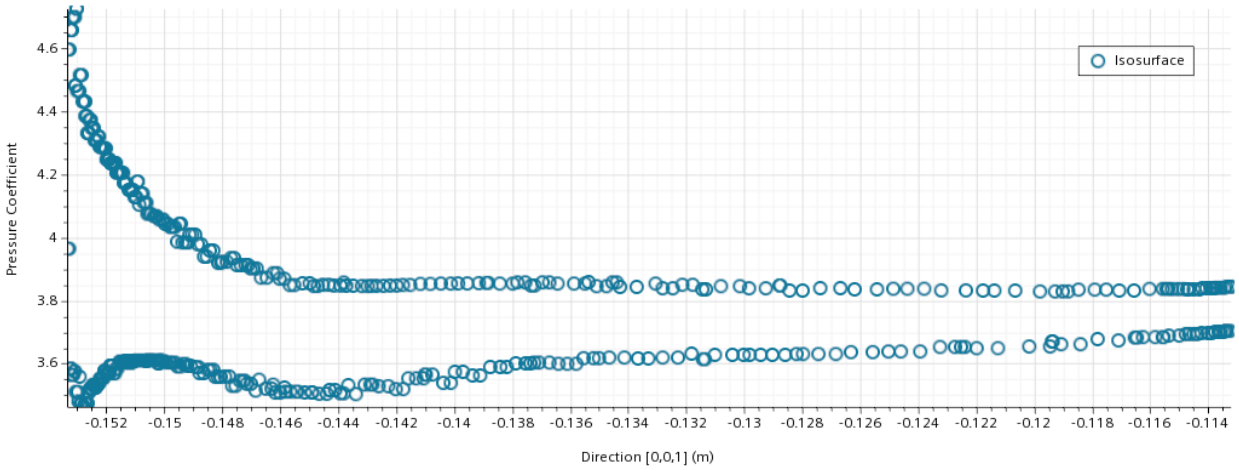

Figure 87: Competition design secondary wing's pressure coefficient distribution along the span at 2.5º of angle of attack

The wake, seen in Figure 88, once again presents the lowest velocity zone behind the fuselage as seen in Figure 83 but it can also be seen a zone of lower velocity corresponding to the secondary wing's span which extends longer in span as in the case of no angle of attack seen in Figure 71.

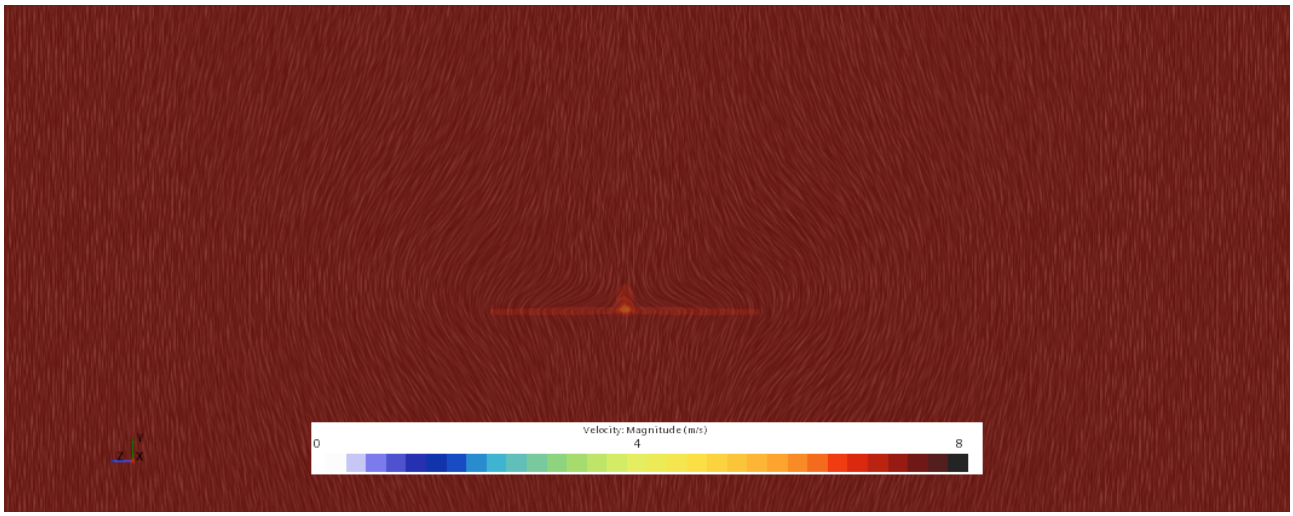

Figure 88: Competition design wake front view velocity contour at 2.5º of angle of attack

When switching to a side point of view, the wake can still be seen behind the fuselage at Figure 89 and also it can be seen how the increase in angle of attack produces a thickening of the boundary layer along the fuselage although there is no detachment, this is seen at the low velocity zone at the upper part of the fuselage. Also, there is a small displacement of the stagnation point in the main wing.

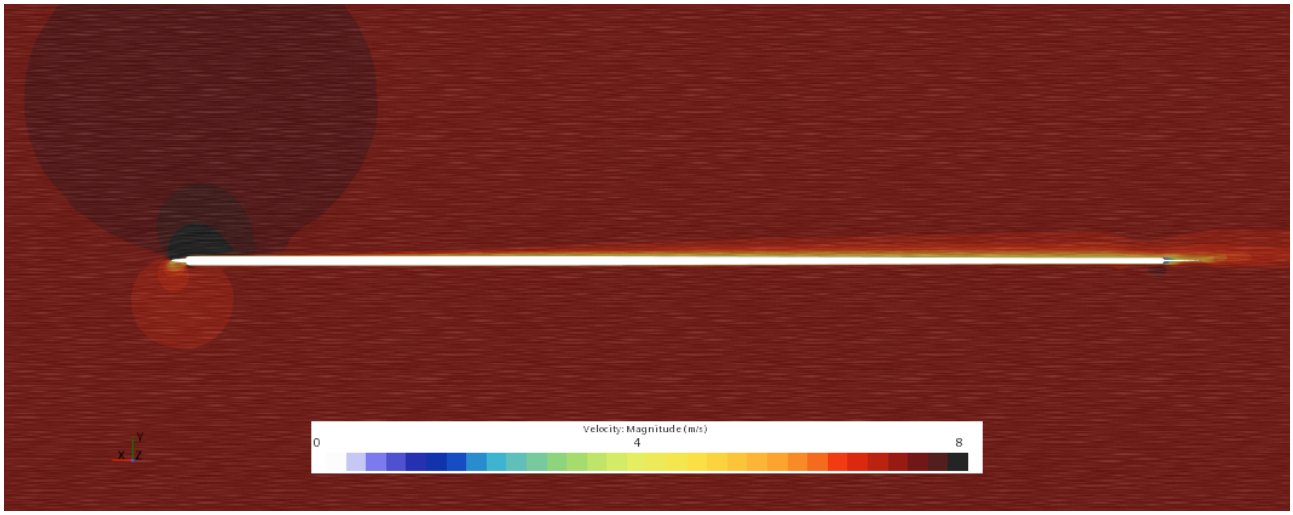

Figure 89: Competition design symmetry view velocity contour at 2.5º of angle of attack

Moving the plane towards the tip, a lower velocity zone can be seen in Figure 90 extending from the lower part of the main wing downstream. The secondary wing shows a slightly higher velocity zone at its top part.

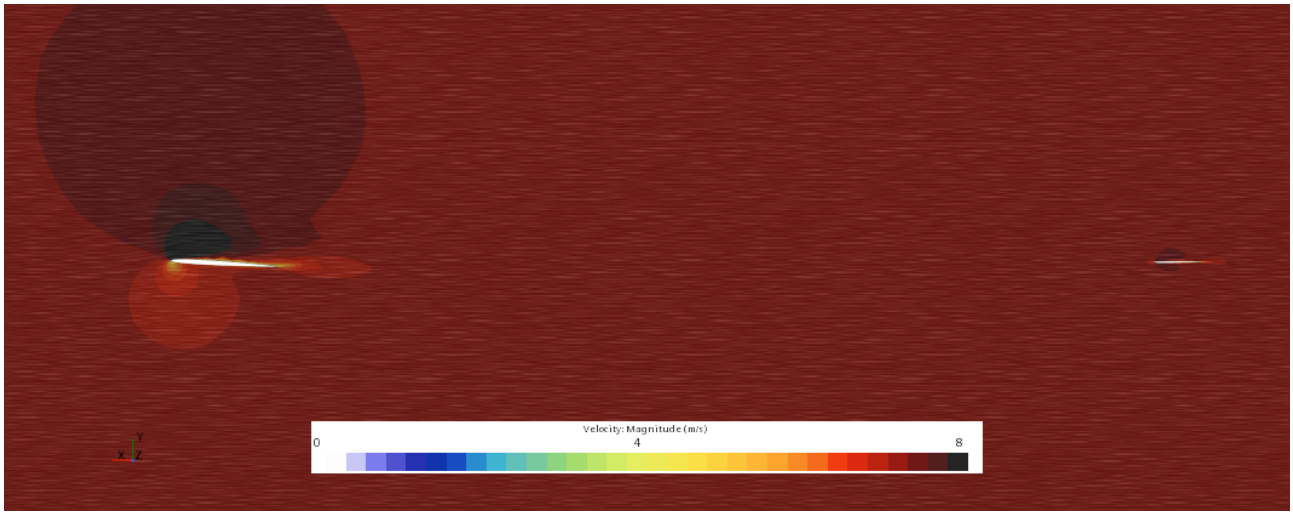

Figure 90: Competition design side view velocity contour at 2.5º of angle of attack

After analyzing the geometry and how it affects the flow at different conditions it can be said that it accomplishes the list of requirements stated for this kind of design. It provides a high pitching moment at any cases studied due to the design of the secondary wing and the fuselage's length, has a small lateral area which provides rolling and yawing maneuverability and is able to reach a velocity high enough to be used in competitive races without having cavitation problems.

7 Conclusions

Along the whole project two different geometries have been designed following different requirements and they have been studied in different scenarios simulating possible real situations in order to analyze their performance and the interaction between the geometries and the fluid.

After performing the aforementioned study, it can been concluded that both of the geometries successfully fulfill all of the requirements established in all of the scenarios studied. For the beginners' design, it shows a stable behaviour and high lift coefficient, providing the pilot all possible facilities to get started in this sport, complementing the lack of experience and ability with the stability provided by the design. In the case of the competition design, it is extremely maneuverable and offers a huge range of velocities before cavitation, providing the pilot with a design that allows him or her to exploit his or her abilities to the fullest and performing at a higher level.

8 Project's Cost, Environmental Impact and Specifications

8.1 Cost

The total cost of the project has been divided into different costs depending on the cause of the cost. Following this criteria, this section is divided into subsections.

8.1.1 Personnel Cost

The personnel cost is the cost related to the employees working in the project, and is summarized in Table 11.

	Time Invested	Cost per time	Total Cost
Author	345 [h]	33 [€/h]	11385 [€]
Tutor	15 [h]	50 [€/h]	750 [€]
		Total cost	**12135 [€]**

Table 11: Personnel cost

8.1.2 Hardware Cost

This section includes the cost related to every hardware needed, as seen in Table 12. The laptop used to carry out this project is a HP and costed 1200€, which is amortized to 10 years [10].

	Time Invested	Cost per time	Total Cost
Laptop	467.5 [h]	0.014[€/h] [€/h]	6.55 [€]
		Total cost	**6.55 [€]**

Table 12: Hardware cost

8.1.3 Software Cost

The cost of the different software needed to develop the project has been estimated in Table 13. For Star CCM+ the power on demand license was used while for Siemens NX and Matlab the free student version was used.

	Time Invested	Cost per time	Total Cost
Microsoft Powerpoint	8 [h]	0 [€/h]	0 [€]
Overleaf	30 [h]	0 [€/h]	0 [€]
Star CCM+	157.5 [h]	0.8 [€/h]	126 [€]
Siemens NX	280 [h]	0 [€/h]	0 [€]
Matlab	2 [h]	0 [€/h]	0 [€]
		Total cost	**126 [€]**

Table 13: Software cost

8.1.4 Energetic and Connection Cost

The energetic cost includes the cost of energetic supply for the hardware used and the internet connection needed (which costs 29.90 € per month), summarized in Table 14 and Table 15.

	Time Invested	Consumption	Cost per time	Total Cost
Laptop's supply	467.5 [h]	0.175 [kW]	0.11 [€/kWh]	9 [€]
Illumination	172.5 [h]	0.015 [kW]	0.11 [€/kWh]	0.28 [€]
			Total cost	**9.28 [€]**

Table 14: Energetic cost

	Time Invested	Cost per time	Total Cost
Internet Connection	35 [h]	0.042 [€/h]	1.47 [€]
		Total cost	**1.47 [€]**

Table 15: Connection cost

8.1.5 Summary and Total Cost

The different costs and the total project's cost are seen in Table 16.

Type of Cost	Value
Personnel	12135 [€]
Hardware	6.55 [€]
Software	126 [€]
Energetic	9.28 [€]
Connection	1.47 [€]
Total cost	**12278.3 [€]**

Table 16: Total project's cost

8.2 Environmental Impact

In order to asses the environmental impact of the project, the 2030 Sustainable Development Goals seen in Table 17 and the project's relation with each one of them are studied.

Sustainable Development Goals (SDGs)	High	Medium	Low	Does Not Apply
SDG 1. **No Poverty**	-	-	-	X
SDG 2. **Zero Hunger**	-	-	-	X
SDG 3. **Good Health and Well-Being**	-	X	-	-
SDG 4. **Quality Education**	-	-	-	X
SDG 5. **Gender Equality**	-	-	-	X
SDG 6. **Clean Water and Sanitation**	-	-	-	X
SDG 7. **Affordable and Clean Energy**	-	-	-	X
SDG 8. **Decent Work and Economic Growth**	-	-	-	X
SDG 9. **Industry, Innovation and Infrastructure**	-	-	-	X
SDG 10. **Reduced Inequalities**	-	-	-	X
SDG 11. **Sustainable Cities and Communities**	-	-	-	X
SDG 12. **Responsible Consumption and Production**	-	-	-	X
SDG 13. **Climate Action**	-	-	-	X
SDG 14. **Life Below Water**	-	-	X	-
SDG 15. **Life on Land**	-	-	-	X
SDG 16. **Peace, Justice and Strong Institutions**	-	-	-	X
SDG 17. **Partnerships for the Goals**	-	-	-	X

Table 17: Table with the estimation of how the performed project is related to the 2030 SDGs.[9]

Due to the purely nautical sporting nature of the project, it can only be related with two of the goals established, since promoting different sports and providing new opportunities to practice them is closely related with the population's good health and well-being but this kind of sport may affect the life below water if is not practiced with the proper responsibility.

8.3 Specifications

This part of the document aims to establish the requirements followed when developing this project. More precisely, and according to Spanish legislation, the regulations established in the Royal Decree 486/1997 and 488/1997 according to the safety and worker's health have been followed. These Decrees establish a series of conditions about the working place dimensions, ergonomics, maintenance and cleanliness, moreover, they also establish conditions for the equipment used such as having a tiltable screen, enough illumination and a large enough working table to ensure proper ergonomics for the worker, all rules followed and taken into consideration when working on the project although it has not been carried out in a professional environment.

In an administrative aspect, the rules established by the Universitat Politècnica de València have been followed, having to submit the project online by means of the university's platform before the 17th of July in order for the tribunal to properly evaluate the project and for defending it between the 21st and 31st of the same month. These deadlines must be followed to ensure a proper evaluation of the project. Apart from the project itself, the presentation that will be used for the defence must be also submitted following the deadliness established.

Lastly, all the documentation generated related to the project which has to be submitted follows the terms and conditions for use and distribution established by the platform Riunet of the Universitat Politècnica de València.

References

[1] Armstrong Foils design

https://www.armstrongfoils.com/ha525-foil-kit/

[2] Gong Foils designs

https://www.gong-galaxy.com/en/product/gong-kite-foil-allvator-v2-x-over-alu-m/

[3] Cabrinha Foils designs

https://www.cabrinha.com/collections/foil-complete-sets/products/0-03-fusion-h-series-kits

[4] Lift Foils designs

https://liftfoils.com/es/efoil

[5] Base Geometry

https://grabcad.com/library/foil-windsurf-1

[6] Kishor G. Nayar, Mostafa H. Sharqawy and John H. Lienhard V. *Seawater thermophysical properties library*

http://web.mit.edu/seawater/2017_MIT_Seawater_Property_Tables_r2b.pdf

[7] NACA airfoil generator.

http://airfoiltools.com/airfoil/naca4digit?MNaca4DigitForm

[8] Global wind atlas

https://globalwindatlas.info/es

[9] United Nations' sustainable development goals

https://sdgs.un.org/goals

[10] Amortization legislation for Spain

https://sede.agenciatributaria.gob.es/Sede/ayuda/manuales-videos-folletos/manuales-practicos/irpf-2021/capitulo-7-rendimientos-actividades-economicas-directa/fase-1-determinacion-rendimiento-neto/amortizaciones-dotaciones-ejercicio-fiscalmente reglas-amortizacion.html

[11] Electricity cost

https://www.omie.es/